Remark. It is possible to construct multiple twins that cannot be treated as a cyclic sequence of binary twin elements. This case occurs if a pair of domain states 1 and 2 are related only by an n-fold rotation or roto-inversion ($n \geq 3$). The resulting coset again contains the alternative twin operations, but in this case *only* for the orientation relation $1 \Rightarrow 2$, and not for $2 \Rightarrow 1$ ('non-transposable' domain pair). This coset procedure thus does not result in a composite group for a domain pair. In order to obtain the composite group, further cosets have to be constructed by means of the higher powers of the twin rotation under consideration. Each new power corresponds to a further domain state and twin law.

This construction leads to a composite symmetry $\mathcal{K}(n)$ of supergroup index $[i] \geq 3$ with respect to the *eigensymmetry* $\mathcal{H}$. This case can occur only for the following $\mathcal{H} \Rightarrow \mathcal{K}$ pairs: $1 \Rightarrow 3$, $\bar{1} \Rightarrow \bar{3}$, $1 \Rightarrow 4$, $1 \Rightarrow \bar{4}$, $m \Rightarrow 4/m$, $1 \Rightarrow 6$, $2 \Rightarrow 6$, $m \Rightarrow \bar{6} = 3/m$, $m \Rightarrow 6/m$, $2/m \Rightarrow 6/m$ (monoaxial point groups), as well as for the two cubic pairs $222 \Rightarrow 23$, $mmm \Rightarrow 2/m\bar{3}$. For the pairs $1 \Rightarrow 3$, $\bar{1} \Rightarrow \bar{3}$, $m \Rightarrow \bar{6} = 3/m$, $2/m \Rightarrow 6/m$ and the two cubic pairs $222 \Rightarrow 23$, $mmm \Rightarrow 2/m\bar{3}$, the $\mathcal{K}$ relations are of index [3] and imply three non-transposable domain states. For the pairs $1 \Rightarrow 4$, $1 \Rightarrow \bar{4}$, $m \Rightarrow 4/m$, as well as $1 \Rightarrow 6$ and $m \Rightarrow 6/m$, four or six different domain states occur. Among them, however, domain pairs related by the second powers of 4 and $\bar{4}$ as well as by the third powers of 6 and $\bar{6}$ operations are transposable, because these twin operations correspond to twofold rotations or, for $\bar{6}$, to m.

No growth twins of this type are known so far. As a transformation twin, langbeinite ($23 \Longleftrightarrow 222$) is the only known example.

3.3.5. Description of the twin law by black–white symmetry

An alternative description of twinning employs the symbolism of colour symmetry. This method was introduced by Curien & Le Corre (1958) and by Curien & Donnay (1959). In this approach, a colour is attributed to each different domain state. Depending on the number of domain states, simple twins with two colours (*i.e.* 'black–white' or 'dichromatic' or 'anti-symmetry' groups) and multiple twins with more than two colours (*i.e.* 'polychromatic' symmetry groups) have to be considered. Two kinds of operations are distinguished:

(i) The symmetry operations of the *eigensymmetry* (point group) of the crystal. These operations are 'colour-preserving' and form the 'monochromatic' *eigensymmetry* group $\mathcal{H}$. The symbols of these operations are unprimed.

(ii) The twin operations, *i.e.* those operations which transform one orientation state into another, are 'colour-changing' operations. Their symbols are designated by a prime if of order 2: $2'$, m', $\bar{1}'$.

For *simple twins*, all colour-changing (twin) operations are binary, hence the two domain states are transposable. The composite symmetry $\mathcal{K}$ of these twins thus can be described by a 'black-and-white' symmetry group. The coset, which defines the twin law, contains only colour-changing (primed) operations. This notation has been used already in previous sections.

It should be noted that symbols such as $4'$ and $6'$, despite appearance to the contrary, represent *binary* black-and-white operations, because $4'$ contains 2, and $6'$ contains 3 and $2'$, with $2'$ being the twin operation. For this reason, these symbols are written here as $4'(2)$ and $6'(3)$, whereby the unprimed symbol in parentheses refers to the *eigensymmetry* part of the twin axis. In contrast, $6'(2)$ would designate a (polychromatic) twin axis which relates three domain states (three colours), each of *eigensymmetry* 2. Twin centres of symmetry $\bar{1}'$ are always added to the symbol in order to bring out an inversion twinning contained in the twin law. In the original version of Curien & Donnay (1959), the black–white symbols were only used for twinning by merohedry. In the present chapter, the symbols are also applied to non-merohedral twins, as is customary for (ferroelastic) domain structures. This has the consequence, however, that the *eigensymmetries* $\mathcal{H}$ or $\mathcal{H}^*$ and the composite symmetries $\mathcal{K}$ or $\mathcal{K}^*$ may belong to different crystal systems and, thus, are referred to different coordinate systems, as shown for the composite symmetry of gypsum in Section 3.3.4.1.

For the treatment of *multiple twins*, 'polychromatic' composite groups $\mathcal{K}(n)$ are required. These contain colour-changing operations of order higher than 2, *i.e.* they relate three or more colours (domain states). Consequently, not all pairs of domain states are transposable. This treatment of multiple twins is rather complicated and only sensible if the composite symmetry group is finite and contains twin axes of low order ($n \leq 8$). For this reason, the symbols for the composite symmetry $\mathcal{K}$ of multiple twins are written without primes; see the examples in Section 3.3.4.4(iii). An extension of the dichromatic twin descriptions to polychromatic symbols for multiple twins was recently presented by Nespolo (2004).

3.3.6. Examples of twinned crystals

In order to illustrate the foregoing rather abstract deliberations, an extensive set of examples of twins occurring either in nature or in the laboratory is presented below. In each case, the twin law is described in two ways: by the coset of alternative twin operations and by the black–white symmetry symbol of the composite symmetry $\mathcal{K}$, as described in Sections 3.3.4 and 3.3.5.

For the description of a twin, the conventional crystallographic coordinate system of the crystal and its *eigensymmetry* group $\mathcal{H}$ are used in general; exceptions are specifically stated. To indicate the orientation of the twin elements (both rational and irrational) and the composition planes, no specific convention has been adopted; rather a variety of intuitively understandable simple symbols are chosen for each particular case, with the additional remark 'rational' or 'irrational' where necessary. Thus, for twin reflection planes and (planar) twin boundaries symbols such as m_x, $m(100)$, $m \parallel (100)$ or $m \perp [100]$ are used, whereas twin rotation axes are designated by 2_z, $2_{[001]}$, $2 \parallel [001]$, $2 \perp (001)$, 3_z, $3_{[111]}$, $4_{[001]}$ *etc.*

3.3.6.1. *Macroscopic identification of twins and of twin laws*

As an introduction to the subsequent examples, this section shows how to recognize and identify twinning in a crystal, either by morphological features and observations in polarized light, or by etching, decoration and X-ray diffraction topography. Diffraction effects of twins are treated in Section 3.3.11.

(i) *Re-entrant angles and twin striations*

The most prominent and easily recognizable morphological features are exhibited by penetration and contact twins with their *re-entrant angles* (*edges*). Re-entrant edges are typical for twins with non-parallel lattices (non-merohedral twins) and reticular merohedral twins with a $\Sigma > 1$ coincidence lattice (*e.g.* $\Sigma 3$ spinel twins). Merohedral $\Sigma 1$ twins with full lattice parallelism in general do not exhibit re-entrant edges but can often be identified by twin-related faces appearing in the morphology of a twinned crystal (*e.g.* $\Sigma 1$ twins of quartz). The re-entrant edges mark the outcrop of the twin boundaries, which are defined by the path of this edge during crystal growth. Note that re-entrant edges occur in any arbitrary intergrowth of crystals, which can sometimes be misinterpreted as twinning.

Illustrations of penetration twins are Figs. 3.3.6.6 ($FeBO_3$), 3.3.6.8 (spinel law, diamond), 3.3.6.15 (staurolite) and 3.3.7.1 (orthoclase feldspar). Contact growth twins with re-entrant angles are presented in Fig. 3.3.6.3 (gypsum) and 3.3.6.7 (calcite). In repeated growth twins (*e.g.* albite, Fig. 3.3.6.13) the parallel re-entrant edges form 'polysynthetic twins'. If the width of the twin lamellae gets smaller and smaller, *twin striations* develop as a characteristic feature of these twins. For further examples see the

sketches in Figs. 335–342 in Phillips (1971), pp. 180–181. A rare case of a merohedral Σ1 twin with re-entrant edges is provided by the inversion growth twins of sodium chlorate $NaClO_3$, which exhibit intergrowths of two opposite {111} tetrahedra (Lan *et al*., 2014).

A prominent example for the morphological identification of twins without re-entrant edges is quartz SiO_2 with its merohedral Σ1 Dauphiné and Brazil twins (*cf*. Section 3.3.6.4). The crucial feature is provided by the trapezohedral facet '*x*' (*cf*. Fig. 3.3.6.5), which appears on the twin partners either in the same (Dauphiné) or mirrored (Brazil) orientation, *cf.* Frondel (1962).

(ii) *Polarized light*

(*a*) *Optical birefringence*. The twinned crystal is placed and rotated between crossed polarizers (*e.g.* on a polarizing microscope). The twin domains are easily recognized by their different optical extinction positions. In favourable cases it is possible to derive orientation relations and the twin law from the angle of rotation between these positions. This method, however, is applicable only for optically anisotropic crystals (*i.e.* not for cubic crystals) and for 'twins with inclined axes'. In twins with parallel lattices (Σ1 merohedral twins) the refractive-index ellipsoids are parallel: hence, all twin components exhibit the same optical extinction position and cannot be distinguished. For Σ1 inversion or reflection twins of enantiomorphic crystals, however, the twin domains may be distinguished by their opposite sense of optical rotation (optical activity, see below). Note that any arbitrary intergrowth of two crystals shows the same birefringence features and should not be misinterpreted as a twin.

Examples of visualization of twin domains by optical birefringence are shown in Figs. 3.3.6.9, 3.3.6.12 and 3.3.7.2 (growth-sector twins), as well as in Figs. 3.3.10.13 and 3.3.10.14 (lamellar transformation twins). Further examples are presented in Figs. 3.4.1.1 and Figs. 3.4.3.7 of the following chapter on domain structures (Chapter 3.4 by Janovec & Přívratská). Another illustrative example is given by Niggli (1942, p. 802, Figs. 583 & 584).

(*b*) *Optical activity*. This method is applicable only to enantiomorphic crystals exhibiting optical activity. The crystal is again placed between crossed polarizers, but now one of the polarizers is rotated alternately in clockwise and anticlockwise directions, whereby the optical extinction positions of the right- and left-handed twin components are (alternately) adopted. Owing to the usually high dispersion of the optical rotation, the use of monochromatic light, which provides a sharply defined extinction, is advised. This method works very well for inversion and reflection twins of optically isotropic crystals (*i.e.* cubic crystals with point groups 23 and 432). An example is the inversion growth twinning of $NaClO_3$ (Lan *et al*., 2014). For optically anisotropic (*i.e*. non-cubic) crystals the effect of birefringence usually dominates and obscures the effect of optical activity, which is recognizable only if the light propagates closely along an optical axis of the crystal. In this way, Brazil twinning in quartz (Frondel, 1962; Gordon, 1945) and gallium phosphate $GaPO_4$ (Engel *et al*., 1989) has been visualized. Another example is shown in Fig. 3.4.3.3 of the following chapter on domain structures (Chapter 3.4 by Janovec & Přívratská). In favourable cases, domains of opposite optical activity can also be distinguished in polarized light propagating perpendicular to an optic axis, *e.g.* in $KLiSO_4$ [point group 6: Klapper *et al*. (1987); Scherf *et al.*, 1997; Klapper *et al*. (2008)]. Further examples are given by Shuvalov & Ivanov (1964) and Koňák *et al*. (1978).

(iii) *Selective surface etching*

Selective chemical etching is an old and powerful tool for revealing the outcrops of crystal defects, such as dislocations, grain boundaries, twin domains and twin boundaries, at the surface of a crystal. The surface is subjected to attack by a suitable liquid (solvent, acid, flux) or gas, which generates an etch pattern that allows one to recognize and identify the defects emerging at the surface. From chemical and physical principles, two different effects are used: (*a*) the selective attack of defects due to the lattice deformations associated with them, and (*b*) the different 'rate of dissolution' of opposite polar faces in pyroelectric (ferroelectric) crystals, which allows the distinction of domains of opposite polarity.

(*a*) *Selective attack of defects*

The etch markings (*e.g*. etch pits of dislocations) on a crystallographic (or artificial) face exhibit shapes and orientations typical for the defect and the face under consideration. If a twin boundary emerges on the face, the etch markings on the two sides of the boundary show different orientations, which – in favourable cases – allows one to identify the twin law. The boundary itself is either visible by an etch groove (if it is accompanied by lattice distortions) or by the line separating regions (domains) with differently oriented etch markings. The most prominent and frequently studied crystal is natural quartz with its Dauphiné ('electrical') and Brazil ('optical') twins (*cf*. Sections 3.3.6.4.1 and 3.3.6.4.2): on artificial (0001) surfaces, etched with hydrofluoric acid, regular triangular etch pits are formed. On both sides of a (usually irregular) Dauphiné boundary these pits are mutually rotated by 180°, according to the twofold twin axis along [001]. On both sides of a Brazil boundary the triangular pits are mirrored across the planes $\{11\bar{2}0\}$ (*i.e.* the twin elements of the Brazil twin; *cf.* Frondel, 1962; Gordon, 1945; Gault, 1949), whereas they are mirrored across $\{10\bar{1}0\}$ for the 'combined law' (Leydolt) twin, *cf.* Section 3.3.6.4.3 and Fig. 3.3.6.4. On (artificial) faces $\{11\bar{2}0\}$ (normal to the twofold *eigensymmetry* axes) the etch pits are essentially diagonal (twofold symmetry), on all other faces they are non-symmetrical. Their orientation is again changed according to the twin law involved. A comprehensive review of the grading of natural quartz crystals for application as radio-frequency stabilizers, using etching and optical activity with particular emphasis on twinning, is presented by Gordon (1945). A study of the growth twinning of quartz-homeotype $GaPO_4$ by etching is given by Engel *et al*. (1989) and Grassl *et al*. (2000).

(*b*) *Etching of antipolar domains*

This method is applicable to pyroelectric crystals (having a unique polar axis), independent of whether they are also ferroelectric or not. These crystals have different growth and, accordingly, different dissolution rates in opposite directions of their polar axis. For example, for ferroelectric lithium niobate $LiNbO_3$ (point group 3*m*) the rate of etching with a mixture of hot HF + HNO_3 is higher on the negative polar side than on the positive one (Niizeki *et al*., 1967; Nassau *et al*., 1965). Thus, on natural or artificial polar faces (*i.e.* not parallel to the polar axis) a typical surface relief is generated by dissolution (etching), revealing the 180° domains emerging from that surface. It consists of elevated and depressed flat regions ('hill-and-valley relief') associated with the polarity of the domains. In addition, etch markings (etch pits) may occur in these regions, which are different in shape and differently oriented in the two regions. Examples of lamellar 180° domains in crystals grown from aqueous solution, revealed by etching with water, are provided by ferroelectric NH_4LiSO_4 (Hildmann, 1980; Jennissen, 1990) and lithium formate monohydrate $LiCOO{\cdot}H_2O$ (Klapper, 1973), both point group *mm*2, and triglycine sulphate (point group 2; Sawada & Abe, 1967). A review of the etching of antipolar domains of various ferroelectric crystals (barium titanate, lithium niobate, triglycine sulphate *etc*.) with their suitable etchants is presented in Tagantsev *et al*. (2010).

(iv) *Surface decoration*

This method reveals the distribution of positive and negative charges on the surface of a body. The first report about this technique goes back to Kundt (1883) and Kundt & Blasius (1886), who dusted a mixture of fine powders of sulphur (yellow) and minium (Pb_3O_4, red) through a small-meshed cotton sieve onto

Table 3.3.6.1. *Types of X-ray reflections generating ('yes') or not generating ('no') X-ray topographic domain contrast (yes/no) for the* $6 \rightarrow 6mm$ *growth twins of* $KLiSO_4$

There are no B2 diffraction cases, because the twin operation does not invert the polarity.

Type of X-ray reflections	Domain contrast (twin diffraction case)
$\{hkil\}$	Yes (B1)
$\{hh\bar{2}hl\}$	No (A)
$\{h0\bar{h}l\}$	No (A)
$\{hki0\}$	Yes (B1)
$\{hh\bar{2}h0\}$	No (A)
$\{h0\bar{h}0\}$	No (A)
$\{000l\}$	No (A)

pyroelectric crystals that had previously been heated or cooled. By this process the sulphur particles are negatively charged and the minium particles are positively charged, and collect on the positive and negative regions of the crystal surface, respectively, thus providing a yellow-and-red picture of the charge distribution. This method also visualizes head-to-head and tail-to-tail boundaries (Fig. 3.3.10.2) emerging from a face parallel to the axis of polarization. Pearson & Feldmann (1958) used a colloidal suspension of sulphur and minium powder in an insulating liquid (hexane) and obtained a higher spatial resolution of ferroelectric domain structures by briefly dipping the crystals into the warmed suspension (*in situ* decoration). Liquid toners for copying apparatus and nematic liquid crystals are also very effective decoration media.

A study of antipolar domains and their boundaries of pyroelectric $KLiSO_4$ (point group 6) using both Kundt's method and a Nashua liquid toner is reported by Klapper *et al.* (1987). Studies of domains in several pyroelectric nitrate crystals with a Xerox toner are presented by Bury and McLaren (1969). A liquid-crystal decoration of ferroelectric domains of triglycine sulphate is shown in Fig. 3.4.1.5 of the following chapter on domain structures (Chapter 3.4 by Janovec & Přívratská). A comprehensive review of the various decoration techniques and their application to the visualization of pyroelectric domain structures is given in Tagantsev *et al.* (2010).

(v) *X-ray diffraction topography*

X-ray diffraction topography with its various techniques is a powerful method for the visualization and characterization of all kinds of crystal defects, among them twins. Two kinds of X-rays are usually applied: *monochromatic radiation* [preferably characteristic $K\alpha$ lines of conventional X-ray tubes, *e.g.* in the technique by Lang (1959)], and *polychromatic ('white') radiation* in the Laue method. The latter has gained worldwide application with the development of synchroton-radiation sources (Tanner & Bowen, 1992; Moore, 1995). X-ray topographs can be obtained by reflections from plane surfaces of bulk crystals (Bragg or reflection case), as well as by transmission through crystal plates with not too high absorption (Laue or transmission case). In the latter method all defects inside the plate are imaged. It is a non-magnifying method, which requires crystals of rather low defect density, allowing mainly dynamical diffraction. Reviews of X-ray topography and its application are given, among others, by Lang (1978, 2004), Tanner (1976), Authier (2001, pp. 513–570) and Baruchel (2004). Pioneering work for the X-ray topographic characterization of twins was done on quartz by Lang (1965, 1967*a*,*b*), Lang & Miuskov (1969) and Phakey (1969). Overviews particularly devoted to twinning are presented by Klapper *et al.* (1983) and Klapper (1987).

X-ray topography is not suitable for twins with inclined axes (non-merohedral twins) because their domains have different lattice orientations and, thus, reflection conditions are usually fulfilled in domains of *only one orientation state*. These twins are more easily and better studied by optical birefringence [*cf.* Section 3.3.6.1(ii)]. For twins by merohedry ($\Sigma = 1$) and reticular merohedry ($\Sigma > 1$), however, all domains of *all orientation states* are exactly in the same reflection position and, thus, simultaneously imaged in one exposure. Two kinds of 'topographic contrast' are used for depicting and characterizing the twin domains: 'structure-factor contrast' (or 'domain contrast') of twin domains and 'boundary contrast' of twin boundaries.

(*a*) *Imaging of domains. Structure-factor (domain) contrast* of twin domains occurs if the twin-related reflections $hkl_{\rm I}$ and $hkl_{\rm II}$ of domains I and II have different structure-factor moduli F, *i.e.* if they belong to twin diffraction case B1 or B2 (*cf.* Klapper & Hahn, 2010): the domains of different orientation states are distinguished by different intensities (different film blackening). Twin-related reflections with equal F moduli (diffraction case A) do not generate domain contrast and are suitable for imaging and characterizing other defects, such as dislocations. Thus it is important to know which reflections belong to diffraction cases A and B1, B2. If the twin law is known or suspected, these cases are easily found as follows: generate the twin composite symmetry by combining the point group of the untwinned crystal and the twin operation, and compare the seven diffraction sets ('face forms') $\{hkl\}$, $\{hhl\}$, $\{h0l\}$ *etc.* of the untwinned and the composite group in Table 10.1.2.2 of ITA (Hahn & Klapper, 2005). If the (names of the) face forms are the same for both groups, the reflection sets belong to diffraction case A, if they are different, to diffraction case B1.

An illustrative example is given by $KLiSO_4$ (room-temperature phase III, point group 6), which exhibits, among others, growth twins with twin law $m \parallel [001]$ and composite point group $6mm$. A comparison of the face forms (reflection sets) of groups 6 and $6mm$ reveals the characteristics of diffraction cases A, B1, B2 of the sets, shown in Table 3.3.6.1. X-ray topographs of this twin are presented in Fig. 3.3.6.1 (Klapper *et al.*, 1987). Another illustrative example is provided by the X-ray topographic study of the III $\rightarrow$ IV phase transition on cooling of $KLiSO_4$: it shows the vanishing of the growth twinning with $m \parallel [001]$ described above *and* the appearance of a new twinning with twofold twin axis 2[001], thus proving the symmetry change from point group 6 of phase III to point group $31m$ of the low-temperature phase IV (Klapper *et al.*, 2008).

(*b*) *Imaging of domain boundaries*. This is essential in such twins by merohedry for which domain contrast does not occur for any of the seven reflection sets. This occurs only for inversion twins of noncentrosymmetric crystals (only B2 diffraction cases are possible), when anomalous scattering is negligible and the F moduli of opposite reflections hkl and $\bar{h}\,\bar{k}\,\bar{l}$ have equal or nearly equal values (obeying Friedel's rule). In such cases, however, the twin boundaries appear by dynamical fringe contrast (corresponding to the *stacking-fault contrast*), provided that the crystal perfection is sufficiently high. An example is shown in Fig. 3.3.6.2.

The dynamical fringe contrast originates from the phase jump of the dynamical X-ray wavefields (*i.e.* of the structure factor) upon crossing the twin boundary. This phase jump may be due to a twin displacement (fault) vector $\mathbf{t}$ (*cf.* Section 3.3.10.4.1). The contrast depends on the component of $\mathbf{t}$ parallel to the diffraction vector $\mathbf{g}$ of the reflection used in the topograph. Thus, by imaging the boundary in several different reflections and analysing the variation of its contrast, the displacement vector can be determined. Details and examples are given in Sections 3.3.10.4.2 and 3.3.10.4.3.

3.3.6.2. *Inversion twins in orthorhombic crystals*

The (polar) 180° twin domains in a (potentially ferroelectric) crystal of *eigensymmetry* $\mathcal{H} = mm2$ $(m_x m_y 2_z)$ and composite symmetry $\mathcal{K} = 2/m\,2/m\,2/m$ (*e.g.* in $KTiOPO_4$, NH_4LiSO_4, lithium formate monohydrate) result from a group–subgroup relation of index $[i] = 2$ with invariance of the symmetry framework (merohedral twins), but antiparallel orientation of the polar

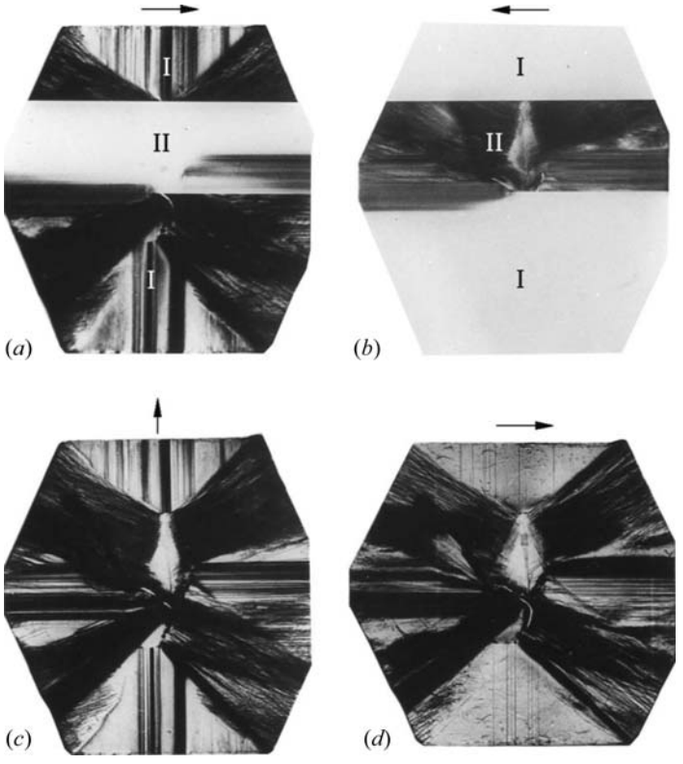

Fig. 3.3.6.1. X-ray topographs (Mo $K\alpha$ radiation) of a $(11\bar{2}0)$ plate (about 12 × 12 mm, about 1 mm thick) cut from a hexagonal $KLiSO_4$ (phase III) crystal (point group 6; *cf.* Klapper *et al.*, 1987), grown from aqueous solution, exhibiting growth reflection twinning of law $m \parallel [001]$ with two domain states I and II. Arrows: diffraction vectors. The twin-related reflections $21\bar{3}0$(I)/$12\bar{3}0$(II) (*a*) and $12\bar{3}0$(I)/$21\bar{3}0$(II) (*b*) (diffraction case B1), with very different moduli $F(12\bar{3}0) = 1.6$ and $F(21\bar{3}0) = 18.2$ (Chung, 1972), map the domain states I and II with very strong domain contrast, which is reversed in (*b*) when the two twin-related reflections are interchanged. The imaging reflections 0003 (*c*) and $30\bar{3}0$ (*d*), both twin diffraction case A, do not reveal the domain states I and II (no domain contrast), but exhibit other growth defects, such as dislocations, faulted growth-sector boundaries *etc*. Note that these defects are not visible in the faintly diffracting domains of (*a*) and (*b*) owing to their small F modulus, which leads to kinematical (*i.e.* extinction-free) diffraction (after Klapper *et al.*, 1987; Klapper & Hahn, 2010).

axes. The orientation relation between the two domain states is described by the coset $k \times \mathcal{H}$ of twin operations shown in Table 3.3.6.2, whereby the reflection in (001), m_z, is considered as the 'representative' twin operation.

Hence, these twins can be regarded not only as reflection, but also as rotation or inversion twins. The composite symmetry, in black–white symmetry notation, is

$$\mathcal{K} = \frac{2'_x}{m_x}\frac{2'_y}{m_y}\frac{2_z}{m'_z}(\bar{1}'),$$

whereby the primed symbols designate the (alternative) twin operations (*cf.* Section 3.3.5).

3.3.6.3. *Twinning of gypsum, $CaSO_4{\cdot}2H_2O$*

The *dovetail twin* of gypsum [*eigensymmetry* $\mathcal{H} = 1\,2/m\,1$, with twin reflection plane $m \parallel (100)$], coset of twin operations $k \times \mathcal{H}$ and composite symmetry $\mathcal{K}$, was treated in Section 3.3.4. Gypsum exhibits an independent additional kind of growth twinning, the *Montmartre twin* with twin reflection plane $m \parallel (001)$. These two twin laws are depicted in Fig. 3.3.6.3. Many colour photographs are presented by Boulliard (2010), pp. 266–271. The two cosets of twin operations in Table 3.3.6.3 and the symbols of the composite symmetries $\mathcal{K}_D$ and $\mathcal{K}_M$ of both twins are referred, in addition to the monoclinic crystal axes, also to orthorhombic axes x_D, y, z_D for dovetail twins and x_M, y, z_M for Montmartre twins. This

Table 3.3.6.2. *Orthorhombic inversion twins: coset of alternative twin operations (twin law)*

$\mathcal{H}$	$k \times \mathcal{H} = m_z \times \mathcal{H}$
1	m_z (normal to the polar axis [001])
m_x	2_x (normal to the polar axis)
m_y	2_y (normal to the polar axis)
2_z	$\bar{1}$ (inversion)

procedure brings out for each case the perpendicularity of the rational and irrational twin elements, clearly visible in Fig. 3.3.6.3, as follows:

$$\mathcal{K}_D = \frac{2'_{xD}}{m'_{xD}}\frac{2_y}{m_y}\frac{2'_{zD}}{m'_{zD}} \qquad \mathcal{K}_M = \frac{2'_{xM}}{m'_{xM}}\frac{2_y}{m_y}\frac{2'_{zM}}{m'_{zM}}$$

x_D (ortho) $\perp$ (100) (mono) $\quad$ x_M (ortho) $\parallel$ [100] (mono)
z_D (ortho) $\parallel$ [001] (mono) $\quad$ z_M (ortho) $\perp$ (001) (mono).

In both cases, the (*eigensymmetry*) framework $2_y/m_y$ is invariant under all twin operations; hence, the composite symmetries $\mathcal{K}_D$ and $\mathcal{K}_M$ are crystallographic of type $2/m\,2/m\,2/m$ (supergroup index [2]) but differently oriented, as shown in Fig. 3.3.6.3. There is no physical reality behind the orthorhombic symmetry of the two $\mathcal{K}$ groups: gypsum is neither structurally nor metrically pseudo-orthorhombic, the monoclinic angle being 128°. The two $\mathcal{K}$ groups and their orthorhombic symbols, however, clearly reveal the two different twin symmetries and, for each case, the perpendicular orientations of the four twin elements, two rational and two irrational. The two twin types originate from independent nucleation in aqueous solutions.

It should be noted that for *all* (potential) twin reflection planes $(h0l)$ in the zone [010] (monoclinic axis), the oriented *eigensymmetry* $\mathcal{H} = 1\,2/m\,1$ would be the same for all domain states, *i.e.* the intersection symmetry $\mathcal{H}^*$ is identical with the oriented

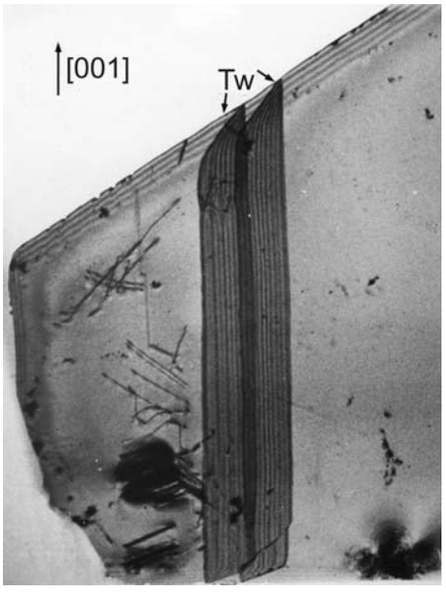

Fig. 3.3.6.2. X-ray transmission topograph of a (110) crystal plate (2.4 mm thick, width about 15 mm) cut from a very perfect crystal of polar lithium formate monohydrate, $HCOOLi{\cdot}H_2O$, point group $mm2$, grown from aqueous solution (reflection 111, Mo $K\alpha$ radiation). The two contrast bands Tw with dynamical interference fringes arise from two (100) inversion-twin lamellae parallel to the polar axis [001]. They have opposite polarity with respect to the bulk crystal and are inclined by 48.3° to the plate surface. The dynamical fringe contrast (stacking-fault contrast) arises from the twin boundaries only, not from the volume of the lamellae (after Klapper, 1973). The interference fringes at the inclined top edge are *Pendellösung* fringes arising from the tapering thickness of the plate.

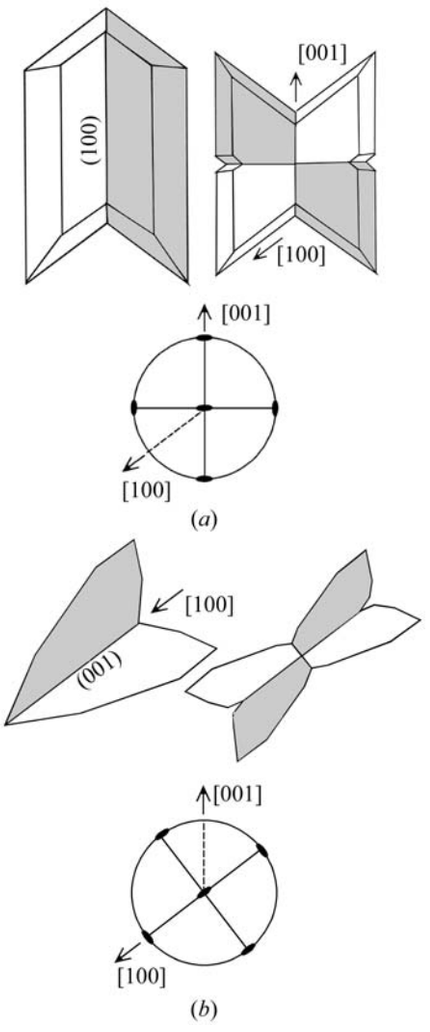

Fig. 3.3.6.3. Dovetail twin (*a*) and Montmartre twin (*b*) of gypsum. The two orientation states of each twin are distinguished by shading. For each twin type (*a*) and (*b*), the following aspects are given: (i) two idealized illustrations of each twin, on the left in the most frequent form with two twin components, on the right in the rare form with four twin components, the morphology of which displays the orthorhombic composite symmetry; (ii) the oriented composite symmetry in stereographic projection (dotted lines indicate monoclinic axes).

eigensymmetry $\mathcal{H}$ and, thus, the composite symmetry would be always crystallographic.

For a more general twin reflection plane not belonging to the zone (*h*0*l*), such as (111), however, the oriented *eigensymmetry* $\mathcal{H}$ would not be invariant under the twin operation. Consequently, an additional twin reflection plane $(1\bar{1}1)$, equivalent with respect to the *eigensymmetry* $12/m1$, exists. This (hypothetical) twin would belong to category (ii) in Section 3.3.4.4 and would formally lead to a noncrystallographic composite symmetry of infinite order. If, however, we restrict our considerations to the intersection symmetry $\mathcal{H}^* = \bar{1}$ of a domain pair, the reduced composite symmetry $\mathcal{K}^* = 2'/m'$ with $m' \parallel (111)$ and $2' \perp (111)$ (irrational) would result. Note that for these (hypothetical) twins the reduced composite symmetry $\mathcal{K}^*$ and the *eigensymmetry* $\mathcal{H}$ are isomorphic groups, but that their orientations are quite different.

Remark. In the domain-structure approach, presented by Janovec & Přívratská in Chapter 3.4 of this volume, both gypsum twins, dovetail and Montmartre, can be derived together as a result of a single (hypothetical) ferroelastic phase transition from a (nonexistent) orthorhombic parent phase of symmetry $\mathcal{G} = 2/m2/m2/m$ to a monoclinic daughter phase of symmetry $\mathcal{H} = 12/m1$, with a very strong metrical distortion of 38° from $\beta = 90°$ to $\beta = 128°$ (Janovec, 2003). In this (hypothetical) transition the two mirror planes, (100) and (001), 90° apart in the orthorhombic form, become twin reflection planes of monoclinic gypsum, (100) for the dovetail, (001) for the Montmartre twin law, with an angle of 128°. It must be realized, however, that neither the orthorhombic parent phase nor the ferroelastic phase transition are real.

3.3.6.4. *Twinning of low-temperature quartz (α-quartz, SiO_2)*

Quartz is a mineral which is particularly rich in twinning. It has the noncentrosymmetric trigonal point group 32 with three polar twofold axes and a non-polar trigonal axis. The crystals exhibit enantiomorphism (right- and left-handed quartz), piezoelectricity and optical activity. The lattice of quartz is hexagonal with holohedral (lattice) point group $6/m\,2/m\,2/m$. Many types of twin laws have been found (*cf.* Frondel, 1962), but only the four most important ones are discussed here:

(*a*) Dauphiné twins;
(*b*) Brazil twins;
(*c*) Combined-law (Leydolt, Liebisch) twins;
(*d*) Japanese twins.

The first three types are merohedral (parallel-lattice) Σ1 twins and their composite symmetries belong to category (i) in Section 3.3.4.2, whereas the non-merohedral Japanese twins (twins with inclined lattices or inclined axes) belong to category (ii).

3.3.6.4.1. *Dauphiné twins*

This twinning is commonly described by a twofold twin rotation around the threefold symmetry axis [001]. The two orientation states are of equal handedness but their polar twofold axes are reversed ('electrical twins'). Dauphiné twins can be transformation or growth or mechanical (ferrobielastic) twins. The composite symmetry is $\mathcal{K} = 622$, the point group of high-temperature quartz (*β*-quartz). The coset decomposition of $\mathcal{K}$ with respect to the *eigensymmetry* $\mathcal{H} = 32$ (index [2]) contains the operations listed in Table 3.3.6.4.

The left coset $2_z \times \mathcal{H}$ constitutes the twin law. Note that this coset contains four twofold rotations of which the first one, 2_z, is the standard description of Dauphiné twinning. In addition, the coset contains two sixfold rotations, 6^1 and $6^5 = 6^{-1}$. The black–white symmetry symbol of the composite symmetry is $\mathcal{K} = 6'(3)22'$ (supergroup of index [2] of the *eigensymmetry* group $\mathcal{H} = 321$).

This coset decomposition $622 \Rightarrow 32$ was first listed and applied to quartz by Janovec (1972, p. 993).

3.3.6.4.2. *Brazil twins*

This twinning is commonly described by a twin reflection across a plane normal to a twofold symmetry axis. The two

Table 3.3.6.3. *Gypsum: cosets of alternative twin operations of the dovetail and the Montmartre twins, referred to their specific orthorhombic axes (subscripts D and M)*

$\mathcal{H}$	Dovetail twins $m_{x\mathrm{D}} \times \mathcal{H}$	Montmartre twins $m_{z\mathrm{M}} \times \mathcal{H}$
1 $2_y = 2 \parallel [010]$ $m_y = m \parallel (010)$ $\bar{1}$	$m_{x\mathrm{D}} = m \parallel (100)$ (rational) $m_{z\mathrm{D}} = m \perp [001]$ (irrational) $2_{z\mathrm{D}} = 2 \parallel [001]$ (rational) $2_{x\mathrm{D}} = 2 \perp (100)$ (irrational)	$m_{z\mathrm{M}} = m \parallel (001)$ (rational) $m_{x\mathrm{M}} = m \perp [100]$ (irrational) $2_{x\mathrm{M}} = 2 \parallel [100]$ (rational) $2_{z\mathrm{M}} = 2 \perp (001)$ (irrational)

Table 3.3.6.4. *Dauphiné twins of α-quartz: coset of alternative twin operations (twin law)*

$\mathcal{H}$	$2_z \times \mathcal{H}$
1	$2_z = 6^3$
3^1	6^5 $(= 6^{-1})$
3^2	6^1
$2_{[100]}$	$2_z \times 2_{[100]} = 2_{[120]}$
$2_{[010]}$	$2_z \times 2_{[010]} = 2_{[210]}$
$2_{[\bar{1}\bar{1}0]}$	$2_z \times 2_{[\bar{1}\bar{1}0]} = 2_{[1\bar{1}0]}$

orientation states are of opposite handedness (*i.e.* the sense of the optical activity is reversed: optical twins) and the polar axes are reversed as well. The coset representing the twin law consists of the following six operations:

(i) three reflections across planes $\{11\bar{2}0\}$, normal to the three twofold axes;

(ii) three rotoinversions $\bar{3}$ around [001]: $\bar{3}^1$, $\bar{3}^3 = \bar{1}$, $\bar{3}^5 = \bar{3}^{-1}$.

The coset shows that Brazil twins can equally well be described as reflection or inversion twins. The composite symmetry

$$\mathcal{K} = \bar{3}'(3)\frac{2}{m'}1(\bar{1}')$$

is a supergroup of index [2] of the *eigensymmetry* group 321.

3.3.6.4.3. *Combined Dauphiné–Brazil (Leydolt, Liebisch) twins*

Twins of this type can be described by a twin reflection across the plane (0001), normal to the threefold axis [001]. The two orientation states of this twin are of opposite handedness (*i.e.* the optical activity is reversed, optical twin), but the polar axes are not reversed. The coset representing the twin law consists of the following six operations:

(i) three twin reflections across planes $\{10\bar{1}0\}$, parallel to the three twofold axes;

(ii) three rotoinversions $\bar{6}$ around [001]: $\bar{6}^1$, $\bar{6}^3 = m_z$, $\bar{6}^5 = \bar{6}^{-1}$.

The composite symmetry

$$\mathcal{K} = \bar{6}'(3)2m' = \frac{3}{m'}2m'$$

is again a supergroup of index [2] of the *eigensymmetry* group 321. This twin law is usually described as a combination of the Dauphiné and Brazil twin laws, *i.e.* as the twofold Dauphiné twin rotation 2_z followed by the Brazil twin reflection $m(11\bar{2}0)$ or, alternatively, by the inversion $\bar{1}$. The product $2_z \times \bar{1} = m_z$ results in a particularly simple description of the combined law as a reflection twin on m_z.

Twin domains of the Leydolt type are very rarely intergrown in direct contact, *i.e.* with a common boundary. If, however, a quartz crystal contains inserts of Dauphiné and Brazil twins, the domains of these two types, even though not in contact, are related by the Leydolt law. In this sense, Leydolt twinning is rather common in low-temperature quartz. In contrast, $GaPO_4$, a quartz homeotype with the berlinite structure, frequently contains Leydolt twin domains in direct contact, *i.e.* with a common boundary (Engel *et al.*, 1989).

In conclusion, the three merohedral twin laws of α-quartz described above imply four domain states with different orientations of important physical properties. These relations are shown in Fig. 3.3.6.4 for electrical polarity, optical activity and the orientation of etch pits on (0001). It is noteworthy that these three twin laws are the only possible merohedral twins of quartz, and that all three are realized in nature. Combined, they lead to the composite symmetry $\mathcal{K} = 6/m\,2/m\,2/m$ ('complete twin': Curien & Donnay, 1959).

In the three twin laws (cosets) above, only odd powers of 6, $\bar{3}$ and $\bar{6}$ (rotations and rotoinversions) occur as twin operations, whereas the even powers are part of the *eigensymmetry* 32.

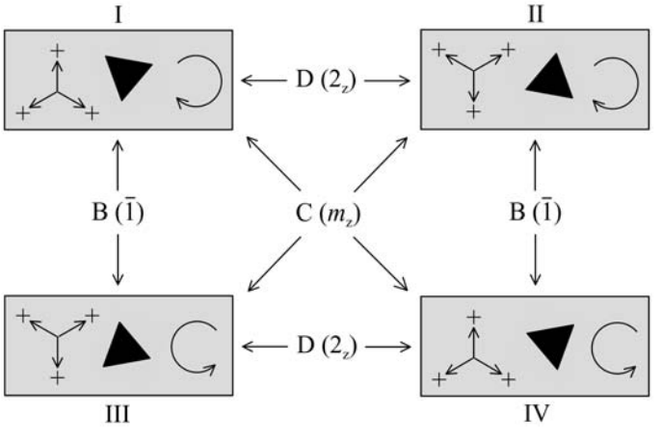

Fig. 3.3.6.4. Distinction of the four different domain states generated by the three merohedral twin laws of low-quartz and of quartz homeotypes such as $GaPO_4$ (Dauphiné, Brazil and Leydolt twins) by means of three properties: orientation of the three electrical axes (triangle of arrows), orientation of etch pits on (001) (solid triangle) and sense of the optical rotation (circular arrow). The twin laws relating two different domain states are indicated by arrows [D (2_z): Dauphiné law; B ($\bar{1}$): Brazil law; C (m_z): Leydolt law]. For $GaPO_4$, see Engel *et al.* (1989).

Consequently, repetition of any odd-power twin operation restores the original orientation state, *i.e.* each of these operations has the nature of a 'binary' twin operation and leads to a pair of *transposable* orientation states.

3.3.6.4.4. *Japanese twins (or La Gardette twins)*

Among the quartz twins with 'inclined axes' ('inclined lattices'), the Japanese twins are the most frequent and important ones. They are contact twins of two individuals with composition plane $(11\bar{2}2)$. This results in an angle of 84°33′ between the two threefold axes. One pair of prism faces is parallel (coplanar) in both partners.

There exist four orientation relations, depending on

(i) the handedness of the two twin partners (equal or different);

(ii) the azimuthal difference (0 or 180°) around the threefold axis of the two partners.

These four variants are illustrated in Fig. 3.3.6.5 and listed in Table 3.3.6.5. The twin interface for all four twin laws is the same, $(11\bar{2}2)$, but only in type III do twin mirror plane and composition plane coincide.

In all four types of Japanese twins, the intersection symmetry (reduced *eigensymmetry*) $\mathcal{H}^*$ of a pair of twin partners is 1. Consequently, the twin laws (cosets) consist of only one twin operation and the reduced composite symmetry $\mathcal{K}^*$ is a group of order 2, represented by the twin element listed in Table 3.3.6.5. If one were to use the full *eigensymmetry* $\mathcal{H} = 32$, the infinite sphere group would result as composite symmetry $\mathcal{K}$.

Many further quartz twins with inclined axes are described by Frondel (1962). A detailed study of these inclined-axis twins in terms of coincidence-site lattices (CSLs) is provided by McLaren (1986) and Grimmer (2006).

3.3.6.5. *Twinning of high-temperature quartz (β-quartz)*

Upon heating quartz into the hexagonal high-temperature phase (point group 622) above 846 K, the Dauphiné twinning disappears, because the composite symmetry $\mathcal{K}$ of the twinned low-temperature phase now becomes the *eigensymmetry* $\mathcal{H}$ of the high-temperature phase. For Brazil twins, however, their nature as reflection or inversion twins is preserved during the transformation.

The *eigensymmetry* of high-temperature quartz is 622 (order 12). Hence, the coset of the Brazil twin law contains 12 twin operations, as follows:

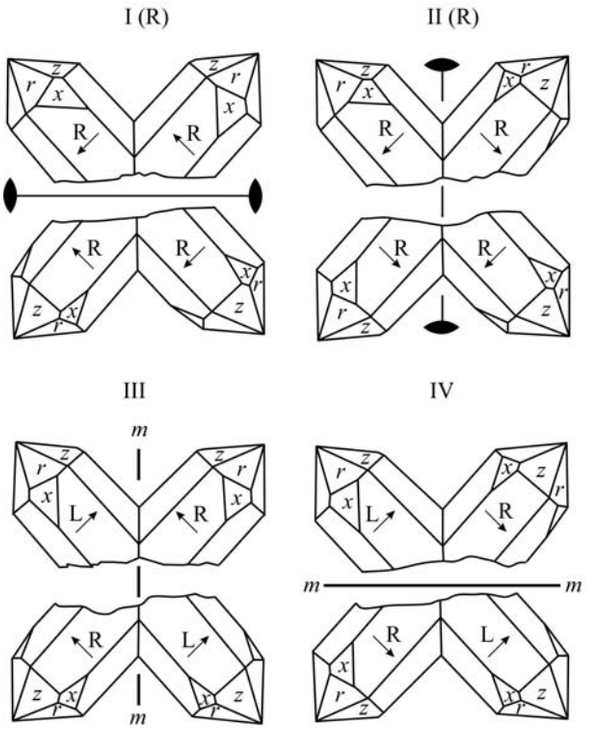

Fig. 3.3.6.5. The four variants of Japanese twins of quartz (after Frondel, 1962; *cf.* Heide, 1928). The twin elements 2 and m and their orientations are shown. In actual twins, either the upper or the lower part of each figure is realized. The lower part has been added for better understanding of the orientation relation. R, L: right-, left-handed quartz. The polarity of the twofold axis parallel to the plane of the drawing is indicated by an arrow. In addition to the cases I(R) and II(R) , I(L) and II(L) also exist, but are not included in the figure. Note that a vertical line in the plane of the figure is the zone axis $[11\bar{1}]$ for the two rhombohedral faces r and z, and is parallel to the twin and composition plane $(11\bar{2}2)$ and the twin axis in variant II.

(i) the six twin operations of a Brazil twin in low-temperature quartz, as listed above in Example 3.3.6.4.2;

(ii) three further reflections across planes $\{10\bar{1}0\}$, which bisect the three Brazil twin planes $\{11\bar{2}0\}$ of low-temperature quartz;

(iii) three further rotoinversions around [001]: $\bar{6}^1$, $\bar{6}^3 = m_z$, $\bar{6}^5 = \bar{6}^{-1}$.

The composite symmetry is

$$\mathcal{K} = \frac{6}{m'}\frac{2}{m'}\frac{2}{m'}(\bar{1}'),$$

a supergroup of index [2] of the *eigensymmetry* 622.

In high-temperature quartz, the combined Dauphiné–Brazil twins (Leydolt twins) are identical with Brazil twins, because the Dauphiné twin operation has become part of the *eigensymmetry* 622. Accordingly, both kinds of twins of low-temperature quartz merge into one upon heating above 846 K. We recommend that these twins are called 'Brazil twins', independent of their type of twinning in the low-temperature phase. Upon cooling below 846 K, transformation Dauphiné twin domains may appear in both Brazil growth domains, leading to the four domain states shown in Fig. 3.3.6.4. Among these four orientation states, two Leydolt pairs occur. Such Leydolt domains, however, are not necessarily in contact (*cf.* Example 3.3.6.4.3 above).

In addition to these twins with 'parallel axes' (merohedral twins), several kinds of growth twins with 'inclined axes' occur in high-temperature quartz. They are not treated here, but additional information is provided by Frondel (1962).

3.3.6.6. *Twinning of rhombohedral crystals*

In some rhombohedral crystals such as corundum Al_2O_3 (Wallace & White, 1967), calcite $CaCO_3$ or $FeBO_3$ (calcite structure) (Kotrbova *et al.*, 1985; Klapper, 1987), growth twinning with a 'twofold twin rotation around the threefold symmetry axis [001]' (similar to the Dauphiné twins in low-temperature quartz described above) is common. Owing to the *eigensymmetry* $\bar{3}2/m$ (order 12), the following 12 twin operations form the coset (twin law). They are described here in hexagonal axes:

(i) three rotations around the threefold axis [001]: 6^1, $6^3 = 2_z$, $6^5 = 6^{-1}$;

(ii) three twofold rotations around the axes [120], [210], $[1\bar{1}0]$;

(iii) three reflections across the planes $(10\bar{1}0)$, $(1\bar{1}00)$, $(01\bar{1}0)$;

(iv) three rotoinversions around the threefold axis [001]: $\bar{6}^1$, $\bar{6}^3 = m_z$ and $\bar{6}^5 = \bar{6}^{-1}$.

Some of these twin elements are shown in Fig. 3.3.6.6. They include the particularly conspicuous twin reflection plane m_z perpendicular to the threefold axis [001]. The composite symmetry is

$$\mathcal{K} = \frac{6'}{m'}(\bar{3})\frac{2}{m}\frac{2'}{m'} \quad \text{(order 24)}.$$

It is of interest that for $FeBO_3$ crystals this twin law always, without exception, forms penetration twins (Fig. 3.3.6.6), whereas for the isotypic calcite $CaCO_3$ only (0001) contact twins are found (Fig. 3.3.6.7). This aspect is discussed further in Section 3.3.8.6. Colour photographs of rhombohedral twins, especially calcite, are provided by Boulliard (2010), pp. 226–238.

3.3.6.7. *Spinel twins*

The twinning of rhombohedral crystals described above also occurs for cubic crystals as the *spinel law* (spinel, CaF_2, PbS, diamond, sphalerite-type structures such as ZnS, GaAs, CdTe, cubic face- and body-centred metals). In principle, all four threefold axes of the cube, which are equivalent with respect to the *eigensymmetry* $\mathcal{H}$, can be active in twinning. We restrict our considerations to the case where only one threefold axis, [111], is involved. The most obvious twin operations are the twofold rotation around [111] or the reflection across (111). For centrosymmetric crystals, they are alternative twin operations and belong to the same twin law. For noncentrosymmetric crystals, however, the two operations represent different twin laws. Both cases are covered by the term 'spinel law'.

The orientation relation defined by the spinel law corresponds to the 'obverse' and 'reverse' positions of two rhombohedra (cubes), as shown in Fig. 3.3.6.8. For the two (differently) oriented *eigensymmetries* $4/m\,\bar{3}\,2/m$ of the domain states $\mathcal{H}_1$ and

Table 3.3.6.5. *The four different variants of Japanese twins according to Frondel (1962)*

Handedness of twin partners	Azimuthal difference (°)	Twin element = twin law	Label in Fig. 65 of Frondel (1962)
L–L or R–R	0	Irrational twofold twin axis normal to plane $(11\bar{2}2)$	I(R), I(L)
	180	Rational twofold twin axis $[11\bar{1}] \equiv [11\bar{2}\bar{3}]$† parallel to plane $(11\bar{2}2)$	II(R), II(L)
L–R or R–L	0	Rational twin mirror plane $(11\bar{2}2)$	III
	180	Irrational twin mirror plane normal to direction $[11\bar{1}] \equiv [11\bar{2}\bar{3}]$†	IV

† The line $[11\bar{1}] \equiv [11\bar{2}\bar{3}]$ is the edge between the faces $z(01\bar{1}1)$ and $r(10\bar{1}1)$ and is parallel to the composition plane $(11\bar{2}2)$. It is parallel or normal to the four twin elements. Transformation formulae between the three-index and the four-index direction symbols, *UVW* and *uvtw*, are given by Barrett & Massalski (1966, p. 13).

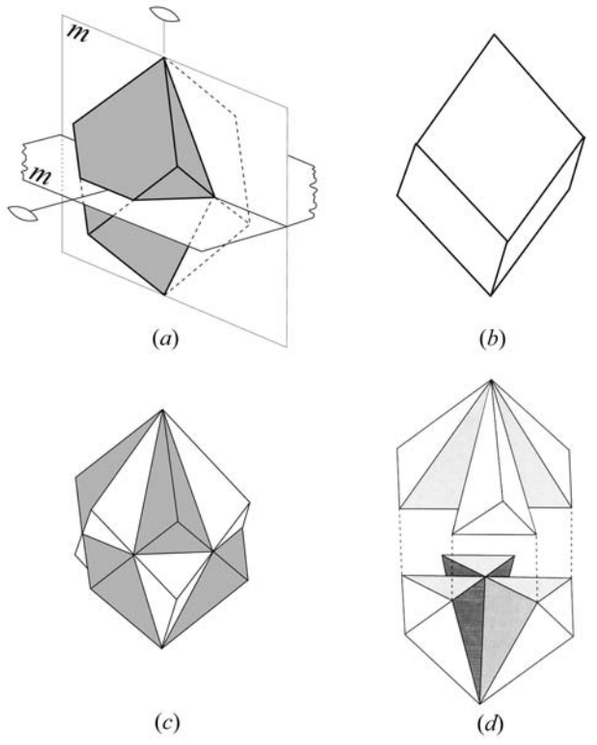

Fig. 3.3.6.6. Twin intergrowth of 'obverse' and 'reverse' rhombohedra of rhombohedral $FeBO_3$. (*a*) 'Obverse' rhombohedron with four of the 12 alternative twin elements. (*b*) 'Reverse' rhombohedron (twin orientation). (*c*) Interpenetration of both rhombohedra, as observed in penetration twins of $FeBO_3$. (*d*) Idealized skeleton of the six components (exploded along [001] for better recognition) of the 'obverse' orientation state shown in (*a*). The components are connected at the edges along the threefold and the twofold *eigensymmetry* axes. The shaded faces are $\{10\bar{1}0\}$ and (0001) coinciding twin reflection and contact planes with the twin components of the 'reverse' orientation state. Parts (*a*) to (*c*) courtesy of R. Diehl, Freiburg.

$\mathcal{H}_2$, the intersection symmetry $\mathcal{H}^* = \bar{3}\,2/m$ (order 12) results. With this 'reduced *eigensymmetry*' $\mathcal{H}^*$, the coset of 12 alternative twin operations is the same as the one derived for twinning of rhombohedral crystals in Example 3.3.6.6.

In the following, we treat the spinel twins with the twin axis [111] or the twin reflection plane (11$\bar{1}$) for the five cubic point groups (*eigensymmetries*) $\mathcal{H} = m\bar{3}m$, $\bar{4}3m$, 432, $m\bar{3}$, 32 in detail. The intersection groups are $\mathcal{H}^* = \bar{3}2/m$, $3m$, 32, $\bar{3}$ and 3, respectively. For these 'reduced *eigensymmetries*', the cosets of the alternative twin operations are listed below with reference to cubic axes.

(*a*) *Eigensymmetry* $\mathcal{H} = 4/m\,\bar{3}\,2/m$ (order 48), reduced *eigensymmetry* $\mathcal{H}^* = \bar{3}2/m1$ (order 12).

Alternative twin operations:

(1) three rotations 6^1, $6^3 = 2$, $6^5 = 6^{-1}$ around the axis [11$\bar{1}$];

(2) three twofold rotations around the axes [11$\bar{2}$], [$\bar{2}$11], [1$\bar{2}$1];

(3) three reflections across the planes (11$\bar{2}$), ($\bar{2}$11), (1$\bar{2}$1);

(4) three rotoinversions around the axis [111]: $\bar{6}^1$, $\bar{6}^3 = m_z$, $\bar{6}^5 = \bar{6}^{-1}$.

Reduced composite symmetry $\mathcal{K}^* = 6'/m'\,(\bar{3})\,2/m\,2'/m'$ (order 24).

(*b*) *Eigensymmetry* $\mathcal{H} = \bar{4}3m$ (order 24), reduced *eigensymmetry* $\mathcal{H}^* = 3m1$ (order 6).

Two different twin laws are possible:

(1) Twin law representative: 'twofold rotation around [111]';

Alternative twin operations: lines (1) and (3) of case (*a*) above;

Reduced composite symmetry: $\mathcal{K}^* = 6'(3)mm'$ (order 12).

(2) Twin law representative: 'reflection across (111)';

Alternative twin operations: lines (2) and (4) of case (*a*) above;

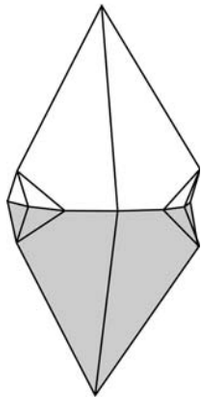

Fig. 3.3.6.7. Contact growth twin of calcite with the same twin law as $FeBO_3$ in Fig. 3.3.6.6. Conspicuous twin element: twin reflection plane (0001), coinciding with the composition plane (0001).

Reduced composite symmetry: $\mathcal{K}^* = \bar{6}'(3)m2' = 3/m'\,m2'$ (order 12).

(*c*) *Eigensymmetry* $\mathcal{H} = 432$ (order 24), reduced *eigensymmetry* $\mathcal{H}^* = 321$ (order 6).

Again, two different twin laws are possible:

(1) Twin law representative: 'twofold rotation around [111]';

Alternative twin operations: lines (1) and (2) of case (*a*) above;

Reduced composite symmetry: $\mathcal{K}^* = 6'(3)22'$ (order 12).

(2) Twin law representative: 'reflection across (111)';

Alternative twin operations: lines (3) and (4) of case (*a*) above;

Reduced composite symmetry: $\mathcal{K}^* = \bar{6}'(3)2m' = 3/m'2m'$ (order 12).

(*d*) *Eigensymmetry* $\mathcal{H} = 2/m\,\bar{3}$ (order 24), reduced *eigensymmetry* $\mathcal{H}^* = \bar{3}$ (order 6).

Two different twin laws:

(1) Twin law representative: 'twofold rotation around [111]' or 'reflection across (111)';

Alternative twin operations: lines (1) and (4) of case (*a*) above;

Reduced composite symmetry: $\mathcal{K}^* = 6'/m'(\bar{3})$ (order 12).

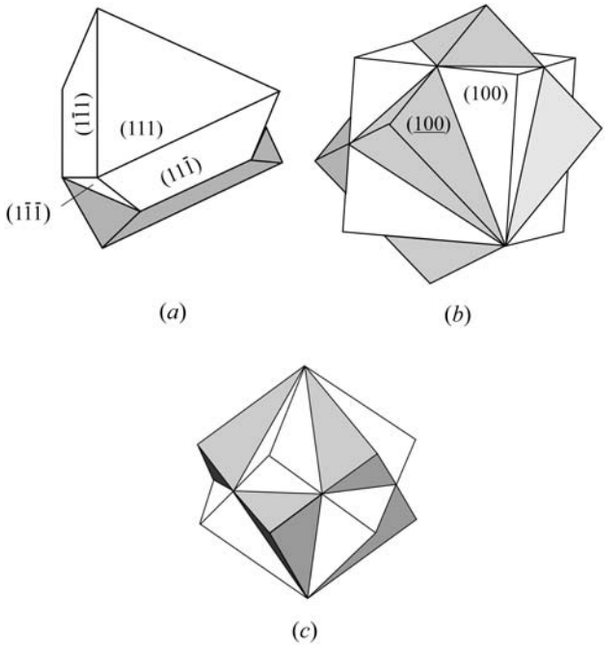

Fig. 3.3.6.8. Spinel (111) twins of cubic crystals (two orientation states). (*a*) Contact twin with (111) composition plane (two twin components). (*b*) and (*c*) Penetration twin (idealized) with one (111) and three $\{11\bar{2}\}$ composition planes (twelve twin components, six of each orientation state) in two different views, (*b*) with one [001] axis vertical, (*c*) with the twin axis [111] vertical.

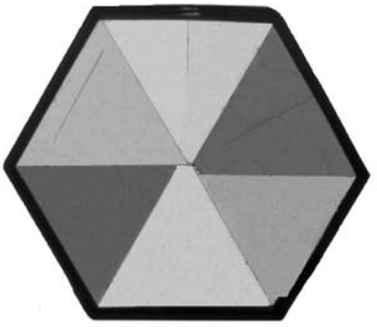

Fig. 3.3.6.9. Pseudo-hexagonal growth twin of K_2SO_4 showing six sector domains in three orientation states. (001) plate, about 1 mm thick and 5 mm in diameter, between polarizers deviating by 45° from crossed position for optimal contrast of all domains. The crystal was precipitated from aqueous K_2SO_4 solution containing 5% S_2O_3 ions. Courtesy of M. Moret, Milano.

(2) Twin law representative: 'reflection across $(11\bar{2})$' or 'twofold rotation around $[11\bar{2}]$';
Alternative twin operations: lines (2) and (3) of case (*a*) above;
Reduced composite symmetry: $\mathcal{K}^* = \bar{3}12'/m'$ (order 12).

(*e*) *Eigensymmetry* $\mathcal{H} = 23$ (order 12), reduced *eigensymmetry* $\mathcal{H}^* = 3$ (order 3).
Four different twin laws are possible:
(1) Twin law representative: 'twofold rotation around [111]';
Alternative twin operations: line (1) of case (*a*) above;
Reduced composite symmetry: $\mathcal{K}^* = 6'(3)$ (order 6).
(2) Twin law representative: 'reflection across (111)'.
Alternative twin operations: line (4) of case (*a*) above.
Reduced composite symmetry: $\mathcal{K}^* = \bar{6}'(3) = 3/m'$ (order 6).
(3) Twin law representative: 'twofold rotation around $[11\bar{2}]$';
Alternative twin operations: line (2) of case (*a*) above;
Reduced composite symmetry $\mathcal{K}^* = 312'$ (order 6).
(4) Twin law representative: 'reflection across $(11\bar{2})$';
Alternative twin operations: line (3) of case (*a*) above;
Reduced composite symmetry: $\mathcal{K}^* = 31m'$ (order 6).

The restriction to only one of the four spinel twin axes ⟨111⟩ combined with the application of the coset expansion to the *reduced eigensymmetry* $\mathcal{H}^*$ always leads to a crystallographic composite symmetry $\mathcal{K}^*$. The supergroup generated from the *full eigensymmetry*, however, would automatically include the other three spinel twin axes and thus would lead to the infinite sphere group $m\overline{\infty}$, *i.e.* would imply infinitely many cosets and (equivalent) twin laws. Higher-order spinel twins are discussed in Section 3.3.8.3. Further details can be found in Klapper & Hahn (2012) Sections 3 and 4, and in Section 3.3.11.4 below.

3.3.6.8. *Growth and transformation twins of K_2SO_4*

K_2SO_4 has an orthorhombic pseudo-hexagonal room-temperature phase with point group $\mathcal{H} = mmm$ and axial ratio $b/a = \tan 60.18°$, and a hexagonal high-temperature phase (> 853 K) with supergroup $\mathcal{G} = 6/m\,2/m\,2/m$. It develops pseudo-hexagonal growth-sector twins with equivalent twin reflection planes (110) and $(1\bar{1}0)$ which are also composition planes, as shown in Fig. 3.3.6.9. As discussed in Sections 3.3.2.3.2 and 3.3.4.4 under (iii), this corresponds to a pseudo-threefold twin axis which, in combination with the twofold *eigensymmetry* axis, is also a pseudo-hexagonal twin axis. The extended composite symmetry is

$$\mathcal{K}(6) = \mathcal{K}(3) = 6(2)/m\,2/m\,2/m.$$

Upon heating above 853 K, the growth-sector twinning disappears. On cooling back into the low-temperature phase, transformation twinning ('domain structure') with three systems of lamellar domains appears. The three orientation states are identical for growth and transformation twins, but the morphology of the twins is not: sectors *versus* lamellae. The composite symmetry $\mathcal{K}$ of the twins at room temperature is the true structural symmetry $\mathcal{G}$ of the 'parent' phase at high temperatures.

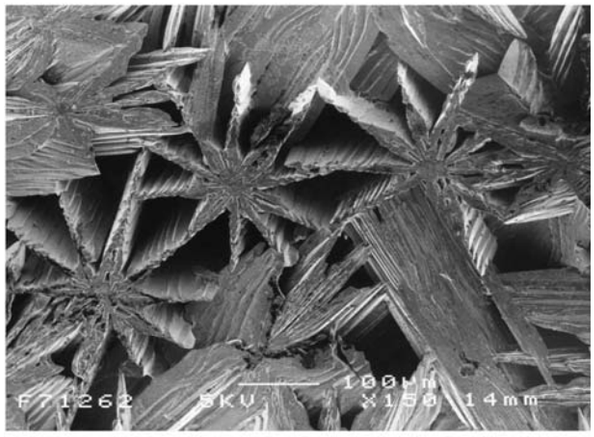

(*a*)

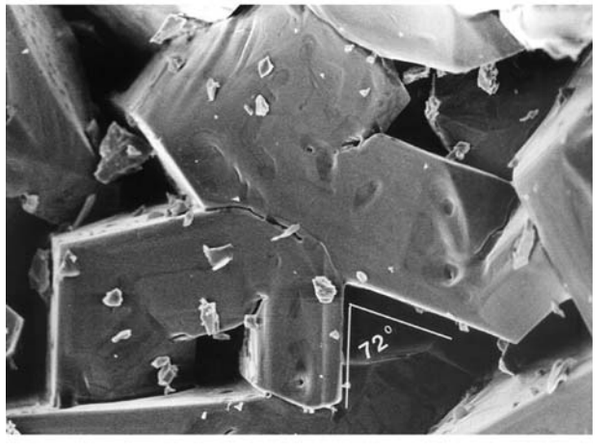

(*b*)

Fig. 3.3.6.10. Pentagonal–decagonal twins. (*a*) Decagonal twins in the shape of tenfold stars on the surface of a bulk alloy, formed during the solidification of a melt of composition $Ru_8Ni_{15}Al_{77}$. Scanning electron microscopy picture. Typical diameter of stars *ca.* 200 µm. The arms of the stars show parallel intergrowth. (*b*) Pentagonal twin aggregate of Fe_4Al_{13} with morphology as grown in the orthorhombic high-temperature phase, showing several typical 72° angles between neighbouring twin partners (diameter of aggregate *ca.* 200 µm). Orthorhombic lattice parameters $a = 7.7510$, $b = 4.0336$, $c = 23.771$ Å, space group *Bmmm*. The parameters c and a approximate the relation $c/a = \tan 72°$; the pseudo-pentagonal twin axis is [010]. On cooling, the monoclinic low-temperature phase is obtained. The twin reflection planes in the orthorhombic unit cell are (101) and $(10\bar{1})$, in the monoclinic unit cell (100) and $(\bar{2}01)$; *cf.* Ellner & Burkhardt (1993, Fig. 10) and Ellner (1995). Both figures courtesy of M. Ellner, Stuttgart.

3.3.6.9. *Pentagonal–decagonal twins*

As was pointed out in Note (6) of Section 3.3.2.4 and in part (iii) of Section 3.3.4.4, there exist twin axes with noncrystallographic multiplicities $n = 5, 7, 8$ *etc.* Twins with five- or tenfold rotations are frequent in intermetallic compounds. As an example, $FeAl_4$ is treated here (Ellner & Burkhardt, 1993; Ellner, 1995). This compound is orthorhombic, $2/m\,2/m\,2/m$, with an axial ratio close to $c/a = \tan 72°$, corresponding to a pseudo-fivefold axis along [010] and equivalent twin mirror planes (101) and $(\bar{1}01)$, which are about 36° apart. In an ideal intergrowth, this leads to a cyclic pseudo-pentagonal or pseudo-decagonal sector twin (Fig. 3.3.6.10). All features of this twinning are analogous to those of pseudo-hexagonal aragonite, treated in Section 3.3.2.3.2, and of K_2SO_4, described above as Example 3.3.6.8.

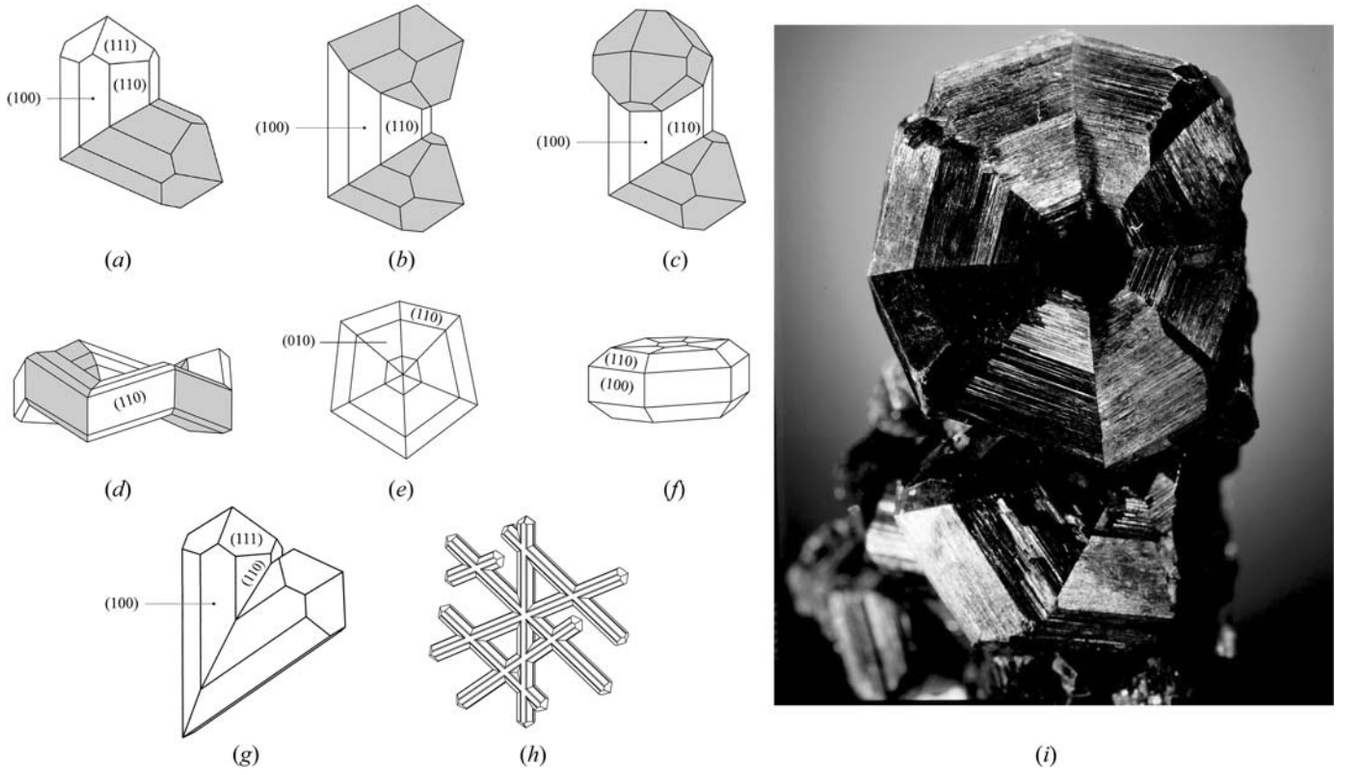

Fig. 3.3.6.11. Various forms of rutile (TiO_2) twins with one or several equivalent twin reflection planes {011}. (*a*) Elbow twin (two orientation states). (*b*) Triple twin (three orientation states) with twin reflection planes (011) and $(0\bar{1}1)$. (*c*) Triple twin with twin reflection planes (011) and (101). (*d*) Cyclic eightfold twin with eight orientation states. (*e*) Cyclic sixfold twin with six orientation states. Two sectors appear strongly distorted due to the large angular excess of 33.6°. (*f*) Perspective view of the cyclic twin of (*e*). (*g*) Twin with reflection plane (031) (heart-shaped twin). (*h*) Sagenite, an intergrowth of (011) twinned rutile (001) prisms. (*i*) Photograph of a rutile eightling (*ca.* 15 mm diameter) from Magnet Cove, Arkansas (Geologisk Museum, Kopenhagen). Parts (*a*) to (*f*) courtesy of H. Strunz, Unterwössen, *cf.* Ramdohr & Strunz, 1967, p. 512. Parts (*g*) and (*h*) courtesy of S. Herting-Agthe (1999), Mineralogical Collections, Technical University Berlin. Photograph (*i*) courtesy of M. Medenbach, Bochum.

The intersection symmetry of all twin partners is $\mathcal{H}^* = 12/m1$; the reduced composite symmetry $\mathcal{K}^*$ of a domain pair in contact is $2'/m'\,2/m\,2'/m'$. The extended composite symmetry of the ideal pentagonal sector twin is $\mathcal{K}(10) = \mathcal{K}(5) = 10'(2')/m'\,2/m\,2'/m'$.

3.3.6.10. *Multiple twins of rutile, TiO_2*

Rutile with *eigensymmetry* $4/m\,2/m\,2/m$ develops growth twins with coinciding twin reflection and composition plane {011}. Owing to its axial ratio $a/c = \tan 57.2°$, the tetragonal c axes of the two twin partners form an angle of 114.4°. The intersection symmetry of the two domains is $\mathcal{H}^* = 2/m$ along the common direction [100]. The reduced composite symmetry of the domain pair is $\mathcal{K}^* = 2/m\,2'/m'\,2'/m'$, with the primed twin elements parallel and normal to the plane (011). A twin of this type, consisting of two domains, is called an 'elbow twin' or a 'knee twin', and is shown in Fig. 3.3.6.11(*a*).

In point group $4/m\,2/m\,2/m$, there exist four equivalent twin reflection planes {011} (four different twin laws) with angles of 65.6° between (001) and $(0\bar{1}1)$ and 45° between (011) and (101), leading to a variety of multiple twins. They may be linear polysynthetic or multiple elbow twins, or any combination thereof (Fig. 3.3.6.11). Very rare are complete cyclic sixfold twins with a large angular excess of $6 \times 5.6° = 33.6°$ (corresponding formally to a '5.5-fold' twin axis) and extended composite pseudosymmetry $\mathcal{K}(6) = 6(2)/m\,2/m\,2/m$, or cyclic eightfold twins with a nearly exact fit of the sectors and a morphological pseudo-$\bar{8}$ twin axis. In the 'sixling', the tetragonal axes of the twin components are coplanar, whereas in the 'eightling' they alternate 'up and down', exhibiting in ideal development the morphological symmetry $\bar{8}2m$ of the twin aggregate. The extended composite symmetry is $\mathcal{K}(8) = 8(1)/m\,2/m\,2/m$ with eight twin components, each of different orientation state. These cyclic twins are depicted in Figs. 3.3.6.11(*d*), (*e*), (*f*) and (*i*).

The sketch of the 'eightling' in Fig. 3.3.6.11(*d*) shows a hole in the centre of the ring, a fact which would pose great problems for the interpretation of the origin of the twin: how do the members of the ring 'know' when to turn and close the ring without any offset? Moreover, the coinciding twin and composition planes {011} in the figures are *not* the growth planes {111} of rutile, *i.e.* all twin boundaries must have been formed already in the nucleus of the twin (*cf.* Section 3.3.7.1.1). Fig. 3.3.6.11(*i*) convincingly shows that the ring is closed at its flat back side (on which the crystal was obviously lying during growth), *i.e.* the growth of all domains started from a central point (nucleus).[3] The open ring in Fig. 3.3.6.11(*d*) is idealized in order to bring out the mutual orientation of the twin components. This seems also to be the case for the other sketches (*b*) and (*c*): here the different domains and the boundaries between them must have started from a common nucleus located in the centre of the half-rings, whereas the sixling in parts (*e*) and (*f*) shows the common nucleus clearly [as well as Fig. 11.13 in the textbook by Klein & Hurlbut (1993, p. 381), and Fig. 10.12 in Berry & Mason (1959, p. 373)].

The (011) rutile twinning treated above is the most frequent one. Another twin, the less frequent (031) reflection twin, usually appears as an intergrowth of two tetragonal prisms in the form of a 'V' (Fig. 3.3.6.11*g*) or of an 'X' with an acute angle of 54.7° and with contact plane (031). 'V'-shaped twins with short 'arms' are often called 'heart'- or 'kite'-shaped twins.

Growth twinning of rutile exhibits a vast variety of complicated (often multiply twinned) forms, the nucleation and growth development of which are in many cases not clear. A well known example is *sagenite* ('reticulated rutile'), a usually pseudo-hexa-

[3] This was confirmed by a special investigation of another 'eightling' from Magnet Cove (Arkansas) by Lieber (2002): the 'eightling' started to grow from the nucleus and developed into the shape of a funnel with an opening of increasing diameter in the centre. This proves the nucleation growth of the ring (*cf.* Section 3.3.7.1.1).

gonal triangular plane grid of intergrown prismatic [001] rods usually twinned on (011), Fig. 3.3.6.11(*h*). The meshes of the grids are often triangles, with two angles of 65.6° [(011) twins] and one angle of 48.8°. The latter angle is enforced by the two prismatic rods in exact (011) twin orientation and does not represent a twin in the strict sense. Rarely also (031) twins occur at a corner of the triangular meshes.

The nucleation and growth history of sagenite is usually based on two observations: free hydrothermal growth, often in the close neighbourhood of quartz (Herting-Agthe, 2009) and by the epitaxial nucleation and growth of prismatic rutile rods with their pseudohexagonal (100) planes on the (0001) planes of hematite or ilmenite (Armbruster, 1981; Force *et al.*, 1996). Interestingly, triangular grids with exactly 60° angles, following the symmetry of the substrate, as well as with angles corresponding to the (011) rutile twin are observed (see also Section 3.3.10.6.2).

The origin of the planar sagenite grid is explained by the epitaxial nucleation and growth of prismatic rutile rods with their (100) planes on the (0001) planes of hematite or ilmenite. The (0001) oxygen layer of hematite is exactly hexagonal, the (100) (undulated) oxygen layer of rutile pseudo-hexagonal, and thus epitactic growth with orientations $(100)_{\rm rut} \parallel (0001)_{\rm hem}$ and $[001]_{\rm rut} \parallel \langle 100\rangle_{\rm hem}$ ('structural coherence': Armbruster, 1981; Force *et al.*, 1996) is suggested. Thus, the rutile rods are nucleated in three orientations and grow together in a triangular arrangement. The hematite substrate is supposed to be dissolved by a later geological process, leaving the sagenite grid. This explanation, however, does not explain the angles of 65.6° and 54.7° between the rutile rods, since the epitaxial nucleation on (0001) hematite would suggest exact 60° angles. This matter deserves further investigation.

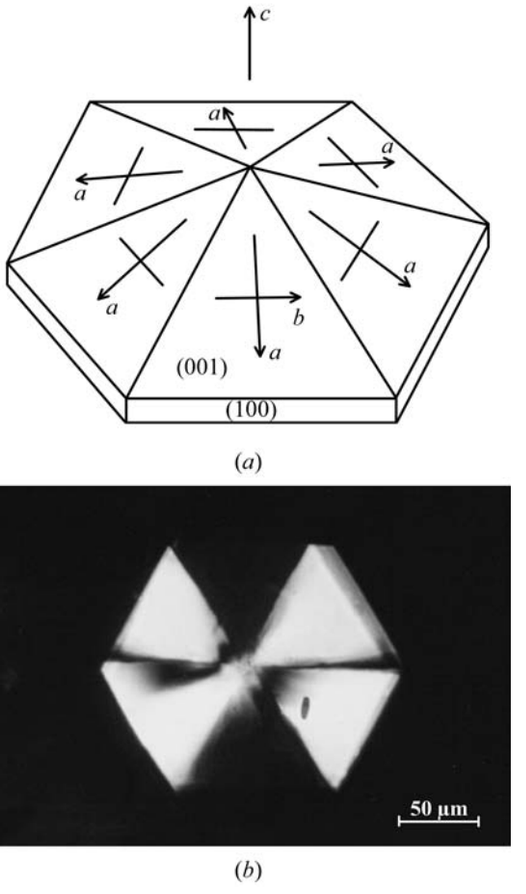

Fig. 3.3.6.12. Sixfold reflection twin of gibbsite, $Al(OH)_3$, with equivalent (110) and $(\bar{1}10)$, both as twin mirror and composition planes. (*a*) Perspective view of a tabular sixfold sector twin with pseudo-hexagonal twin axis *c*. In each sector the monoclinic *b* axis is normal to the twin axis *c*, whereas the *a* axis slopes slightly down by about 4.5° ($\beta = 94.5°$), leading to an umbrella-like shape of the twin. (*b*) Polarization micrograph of a sixfold twinned hexagon (six orientation states) of the shape shown in (*a*). Pairs of opposite twin components have the same optical extinction position. Courtesy of Ch. Sweegers, PhD thesis, University of Nijmegen, 2001.

3.3.6.11. *Variety of twinning in gibbsite, $Al(OH)_3$*

Gibbsite (older name: hydrargillite) forms a pronounced layer structure with a perfect cleavage plane (001). It is monoclinic with *eigensymmetry* $\mathcal{H} = 12/m1$, but strongly pseudo-hexagonal in (001) with an axial ratio $b/a = \tan 30.4°$. In contrast to most other pseudo-hexagonal crystals, the twofold *eigensymmetry* axis *b* is not parallel but normal to the pseudo-hexagonal *c* axis. The normal to the cleavage plane (001) is inclined by $\beta - 90° = 4.5°$ against [001]. Owing to the pseudo-hexagonal metrics of the plane (001), the lattice planes (110) and $(\bar{1}10)$, equivalent with respect to the *eigensymmetry* $\mathcal{H} = 2/m$, form an angle of 60.8°.

The following four significant twin laws have been observed by Brögger (1890):

(i) *(001) reflection twin*: the cleavage plane (001) acts both as twin mirror and composition plane. The pseudo-hexagonal axes [001] of both partners are inclined to each other by 9.0°. This twin law is quite common in natural and synthetic gibbsite.

(ii) *(100) reflection twin*: the twin mirror plane (100) is also the composition plane. The angle between the (001) planes of both partners is 9.0°, as in (i); the pseudo-hexagonal axes [001] of both partners are parallel. This twin law is not common.

(iii) *(110) reflection twin*: again, twin mirror plane and composition plane coincide. The two (001) planes span an angle of 4.6°. This twin law is very rare in nature, but is often observed in synthetic materials. A sixfold sector twin of synthetic gibbsite, formed by cyclic repetition of {110} twin reflection planes 60.8° apart, is shown in Fig. 3.3.6.12. The pseudo-hexagonal axis [001] is common to all domains. Since the (001) plane is inclined towards this axis at 94.5°, the six (001) facets of the twinned crystal form a kind of 'umbrella' with [001] as umbrella axis (Fig. 3.3.6.12*a*). This (001) umbrella faceting was recently observed in twinned synthetic gibbsite crystals by Sweegers *et al.* (1999).

In contrast to orthorhombic aragonite with only three pseudo-hexagonal orientation states, these gibbsite twins exhibit *six* different orientation states. This is due to the absence of any *eigensymmetry* element along the pseudo-hexagonal axis [001]. The intersection symmetry of all orientation states is $\bar{1}$. The reduced composite symmetry of a domain pair is $\mathcal{K}^* = 12'/m'1$, with m' the twin mirror plane (110).

(iv) '*Median law*': According to Brögger (1890), this twin law implies exact parallelism of non-equivalent edges $[110]_{\rm I}$ and $[010]_{\rm II}$, and *vice versa*, of partners I and II. The twin element is an irrational twofold axis parallel to (001), bisecting *exactly* the angle between [110] and [010], or alternatively, an irrational twin reflection plane normal to this axis. This interesting orientation relation, which has been observed so far only for gibbsite, does not obey the minimum condition for twinning as set out in Section 3.3.2.2. An alternative interpretation, treating these twins as *rational* [130] rotation twins, is given by Johnsen (1907), *cf.* Tertsch (1936), pp. 483–484. Interestingly, this strange 'twin law' is the most abundant one among natural gibbsite twins.

3.3.6.12. *Plagioclase twins*

From the point of view of the relationship between pseudo-symmetry and twinning, triclinic crystals are of particular interest. Classical mineralogical examples are the plagioclase feldspars with the 'albite' and 'pericline' twin laws of triclinic (crystal class $\bar{1}$) albite $NaAlSi_3O_8$ and anorthite $CaAl_2Si_2O_8$ (also microcline, triclinic $KAlSi_3O_8$), which all exhibit strong pseudosymmetries to the monoclinic feldspar structure of sanidine. Microcline undergoes a very sluggish monoclinic–triclinic phase transformation involving Si/Al ordering from sanidine to microcline, whereas

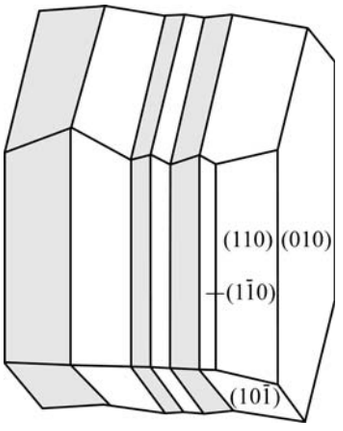

Fig. 3.3.6.13. Polysynthetic albite twin aggregate of triclinic feldspar, twin reflection and composition plane (010).

albite experiences a quick, displacive transformation from monoclinic monalbite to triclinic albite.

The composite symmetries of these triclinic twins can be formulated as follows:

Albite law: reflection twin on (010); composition plane (010) rational (Fig. 3.3.6.13, Table 3.3.6.6). $\mathcal{K}_A = 2'/m'(\bar{1})$ with rational $m' \parallel (010)$.

Pericline law: twofold rotation twin along [010]; composition plane irrational $\parallel$ [010]: 'rhombic section' (Fig. 3.3.6.14, Table 3.3.6.6). $\mathcal{K}_P = 2'/m'(\bar{1})$ with rational $2' \parallel [010]$.

Both twin laws resemble closely the monoclinic pseudosymmetry $2/m$ in two slightly different but distinct fashions: each twin law $\mathcal{K}$ uses one rational twin element from $2/m$, the other one is irrational. The two frameworks of twin symmetry $2'/m'$ are inclined with respect to each other by about 4°, corresponding to the angle between b (direct lattice) and b^* (reciprocal lattice).

Both twins occur as growth and transformation twins: they appear together in the characteristic lamellar 'transformation microclines'. Details of feldspar twins are given in Smith (1974).

3.3.6.13. *Staurolite*

The mineral staurolite, which has the approximate formula $Fe_2Al_9[O_6(O,OH)_2/(SiO_4)_4]$, has 'remained an enigma' (Smith, 1968) to date with respect to the subtle details of symmetry, twinning, structure and chemical composition. A lively account of these problems is provided by Donnay & Donnay (1983). Staurolite is strongly pseudo-orthorhombic, *Ccmm*, and only detailed optical, morphological and X-ray experiments reveal monoclinic symmetry, $C12/m1$, with $a = 7.87$, $b = 16.62$, $c = 5.65$ Å and $\beta = 90°$ within experimental errors (Hurst *et al.*, 1956; Smith, 1968; and especially Hawthorne *et al.*, 1993).

Staurolite exhibits two quite different kinds of twins:

(i) *Twinning by high-order merohedry* (after Friedel, 1926, p. 56) was predicted by Hurst *et al.* (1956) in their detailed study of staurolite twinning. Staurolite crystals are supposed to consist of very fine scale monoclinic ($\mathcal{H} = 12/m1$) microtwins on m(001), which yield a twin aggregate of orthorhombic composite symmetry $\mathcal{K} = 2'/m'\,2/m\,2'/m'$. The coset consists of m'(001), m'(100), $2' \parallel [100]$ and $2' \parallel [001]$. Even though this twinning appears highly probable due to the pronounced structural pseudosymmetry ('high-order merohedry') of staurolite and has been mentioned by several authors (*e.g.* Smith, 1968), so far it has never been unambiguously proven. In particular, electron-microscopy investigations by Fitzpatrick (1976, quoted in Bringhurst & Griffin, 1986, p. 1470) have failed to detect the submicroscopic twins.

(ii) Superimposed upon this first generation of microtwins very often occurs one or the other of *two spectacular 'macroscopic' growth penetration twins* in the shape of a cross, from which in 1792 the name 'stauros' of the mineral was given by Delamétherié. The first detailed analysis of these twins was provided by Friedel (1926, p. 461). For pictures see Boulliard (2010), p. 264.

Table 3.3.6.6. *Plagioclase: albite and pericline twins*

$\mathcal{H}$	$k \times \mathcal{H}$ (albite)	$k \times \mathcal{H}$ (pericline)
1	$m \parallel (010)$ rational	$2 \parallel [010]$ rational
$\bar{1}$	$2 \perp (010)$ irrational	$m \perp [010]$ irrational

(*a*) The *90° cross* (*Greek cross*) with twin reflection and composition plane (031) is illustrated in Fig. 3.3.6.15(*a*) [*cf.* also the figures on p. 151 of Hurst *et al.* (1956) for less idealized drawings]. Plane (031) generates two twin components with an angle of $2\arctan(b/3c) = 2\arctan 0.9805 = 88.9°$, very close to 90°, between their c axes. The equivalent twin reflection plane $(0\bar{3}1)$ leads to the same angle, and both twin planes intersect along the lattice row [100].

With *eigensymmetry* $\mathcal{H} = 12/m1$, the intersection symmetry of the domain pair is $\mathcal{H}^* = \bar{1}$ and the reduced composite symmetry is $\mathcal{K}^* = 2'/m'$ [$m' = (031)$]. Owing to the special axial ratio $b/3c \approx 1$ mentioned above, the 90° cross is an excellent example of a pseudo-tetragonal twin. The extended composite symmetry of this twin is oriented along [100]:

$$\mathcal{K}(4) = 4(2)/m\,2/m\,2/m$$

[*cf.* Section 3.3.4.2(iii)] with two domain states and all twin operations binary.

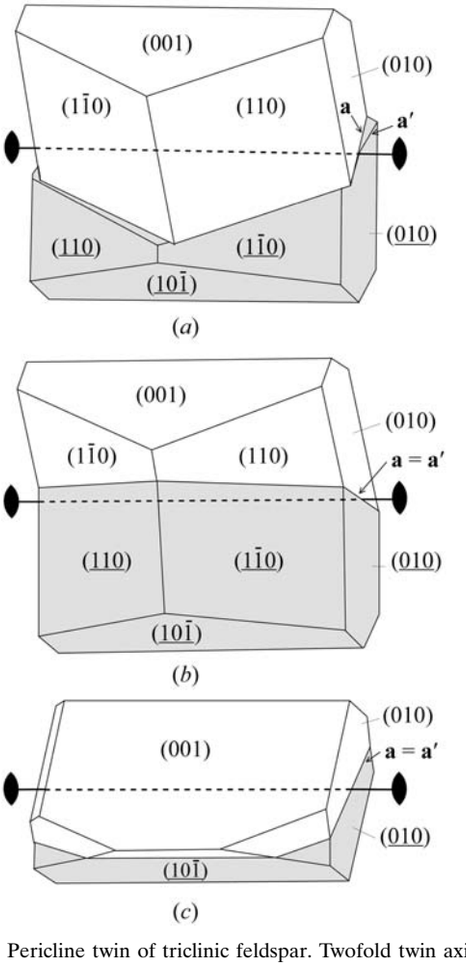

Fig. 3.3.6.14. Pericline twin of triclinic feldspar. Twofold twin axis [010]. (*a*) Twin with rational composition plane (001), exhibiting clearly the misfit (exaggerated) of the two adjacent (001) contact planes, as indicated by the crossing of lines **a** and **a**′. (*b*) The same (exaggerated) twin as in (*a*) but with irrational boundary along the 'rhombic section': fitting of contact planes from both sides (**a** and **a**′ coincide and form a flat ridge). (*c*) Sketch of a real pericline twin with irrational interface ('rhombic section') containing the twin axis.

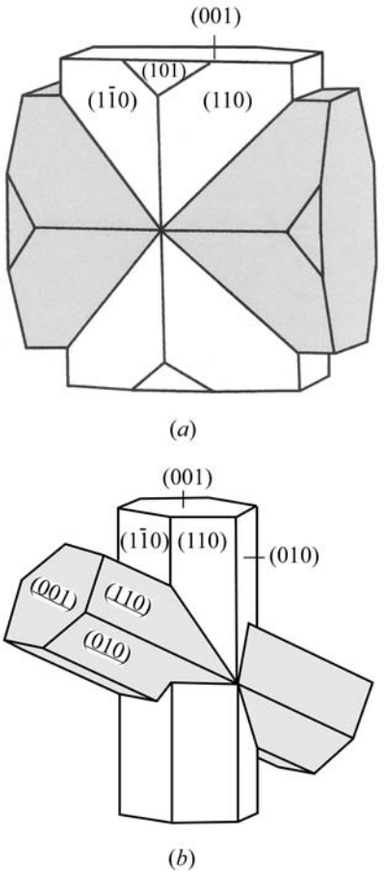

Fig. 3.3.6.15. Twinning of staurolite. (*a*) 90° cross ('Greek cross') with twin reflection and composition planes (031) and (03$\bar{1}$). (*b*) 60° cross ('St Andrew's cross') with twin reflection and composition plane (231).

(*b*) The *60° cross* (*St Andrew's cross*) with twin reflection plane (231) is illustrated in Fig. 3.3.6.15(*b*). It is the more abundant of the two crosses, with a ratio of 60°:90° twins $\approx$ 9:1 in one Georgia, USA, locality (*cf.* Hurst *et al.*, 1956, p. 152). Two equivalent twin mirror planes, (231) and (2$\bar{3}$1), intersecting in lattice row [10$\bar{2}$] exist. They include an angle of 60.4°. The action of one of these twin reflection planes leads to the 60° cross with an angle of 60° between the two *c* axes. The reduced composite symmetry of this twin pair is $\mathcal{K}^* = 2'/m'$ [$m' = (231)$].

In rare cases, penetration trillings occur by the action of *both* equivalent mirror planes, (231) and (2$\bar{3}$1), leading to three interpenetrating twin components with angles of about 60° between neighbouring arms.

Notes

(1) In many books, the twin reflection planes for the 90° cross and the 60° cross are given as (032) and (232) instead of (031) and (231). The former Miller indices refer to the morphological cell, which has a double *c* axis compared with the structural X-ray cell, used here.

(2) Friedel (1926) and Hurst *et al.* (1956) have derived both twin laws (031) and (231), mentioned above, from a multiple cubic pseudo-cell, the 'Mallard pseudo-cube'. This derivation will be presented in Section 3.3.9.2.4 as a characteristic example of 'twinning by reticular pseudo-merohedry'.

(3) A very similar twinning situation, including the use of a pseudo-cube, has been reported for the monoclinic ($P2_1/n$) pseudo-cubic mineral cryolite, Na_3AlF_6, by Donnay (1952) and Wrinch (1952).

3.3.6.14. *$BaTiO_3$ transformation twins*

The perovskite family, represented by its well known member $BaTiO_3$, is one of the technically most important groups of dielectric materials, characterized by polar structures which exhibit piezoelectricity, pyroelectricity and, most of all, ferroelectricity.

$BaTiO_3$ is cubic and centrosymmetric (paraelectric) above 393 K. Upon cooling below this temperature it transforms in one step (first-order transformation with small ΔH) into the ferroelectric tetragonal phase with polar space group *P*4*mm*. This transition is *translationengleich* of index $[i] = 6$. Hence there are domains of six possible orientation states at room temperature. The transformation can be theoretically divided into two steps:

(i) *Translationengleiche* symmetry reduction cubic $Pm\bar{3}m \longrightarrow$ tetragonal $P4/mmm$ of index $[i_1] = 3$, leading to three sets of *ferroelastic* '90° domains', related by the (lost) cubic {110} twin mirror planes or the (lost) cubic threefold axes. These three pseudo-merohedral orientation states point with their tetragonal *c* axes along the three former cube axes [100], [010] and [001], thus including angles of nearly 90°.

(ii) Each of these centrosymmetric domains splits into two *antiparallel* polar ferroelectric '180° domains', whereby the space group $P4/mmm$ is *translationsgleich* reduced to *P*4*mm* of index $[i_2] = 2$. The total index is: $[i] = [i_1] \cdot [i_2] = 6$.

The beautiful polysynthetic twin structure of $BaTiO_3$ is shown in the colour micrograph Fig. 3.4.1.1 in Chapter 3.4 of this volume.

3.3.6.15. *Merohedral growth twinning of pentaerythrite*

Crystals of pentaerythrite (PE), $C(CH_2OH)_4$, grown from solutions in water or a water/ethanol mixture, exhibit nearly without exception twinning by merohedry. This is already indicated by its predominantly tetragonal bi-pyramidal morphology (Ernst, 1928), which is not compatible with the point group $\bar{4}$ (space group $I\bar{4}$) of the single crystal. The point group $\bar{4}$ allows three merohedral twin laws:

(*a*) m'(001), composite symmetry $4/m'$ (inversion twin $\bar{1}'$);

(*b*) m'(100), composite symmetry $\bar{4}m'2'$;

(*c*) m'(110), composite symmetry $\bar{4}2'm'$.

Of special interest are here the laws (*b*) and (*c*), which lead to two different structural settings and are, thus, different twin laws. Since the predominant growth face of PE is the tetragonal sphenoid (tetragonal tetrahedron) (111) (Groth, 1910), all three twin elements generate the tetragonal bi-pyramid {111} (pseudo-cubic octahedron) in their composite symmetry, as is actually observed.

A detailed analysis of the growth twinning of PE has been reported by Renninger (1957). He identified the inversion twinning by studying (001) cleavage plates by polarization optics. These generally exhibit four regions, corresponding to the four pyramid growth sectors, of different optical behaviour. This, however, is due to a pronounced 'optical anomaly' (*cf.* 'Extended note' in Section 3.3.1 above), here by a biaxial splitting of the optical axis of up to 8°, and not by a reversal of optical rotation, which does not exist along a $\bar{4}$ axis. Twin laws (*b*) or (*c*) were identified by the intensity interchange of twin-related reflections (*hkl*) and (*khl*) on Laue diffraction patterns. This was confirmed by a rather unusual method, by rocking curves of (130)–(310) reflections (having very different structure-factor moduli) on both sides of a (*b*) or (*c*) twin boundary. The X-ray methods, however, could not distinguish between twin laws (*b*) and (*c*). This is possible by the different mutual orientations of etch pits on (001) cleavage planes on both sides of the twin boundaries [*cf.* Section 3.3.6.1(iii)(*a*)].

3.3.6.16. *Twins of twins*

This term is due to Henke (2003) and refers to the simultaneous occurrence (superposition) of two or more different twin types (twin laws) in one and the same crystal. In *twins of twins*, one 'generation' of twin domains is superimposed upon the

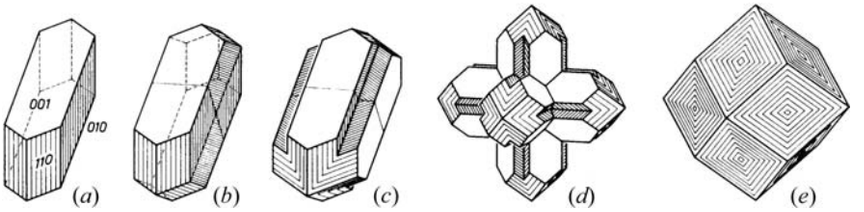

Fig. 3.3.6.16. The various steps (idealized) of phillipsite growth twins: (*a*) monoclinic untwinned, (*b*) orthorhombic, (*c*) tetragonal, (*d*) cubic, and (*e*) 'filled-in' pseudo rhomb-dodecahedron (after Ramdohr & Strunz, 1967, p. 754).

other, each with its own twin law. This may occur as a result of:

(1) two successive phase transitions, each with its own twinning scheme, or

(2) one phase transition with loss of two kinds of symmetry elements, or

(3) a phase transition superimposed on an existing growth twin.

Typical examples are:

(i) the cubic–tetragonal ($m\bar{3}m \Longleftrightarrow 4mm$) phase transition of $BaTiO_3$, described above. Here, 90° domains (due to the loss of the diagonal mirror planes) are superimposed by 180° domains (due to the loss of the inversion centres);

(ii) a similar case (tetragonal–monoclinic) is provided by the 'type case' of Henke (2003), $(NO)_2VCl_6$;

(iii) ammonium lithium sulfate exhibits pseudo-hexagonal growth-sector twins upon which lamellae of ferroelectric 180° domains are superimposed (Hildmann, 1980; Jennissen, 1990).

In this context, the term *complete twin* should be noted. It was coined by Curien & Donnay (1959) for the symmetry description of a crystal containing several merohedral twin laws. Their preferred example was quartz, but there are many relevant cases:

(i) The complete merohedral 'twins of twins' of quartz, *i.e.* the superposition of the Dauphiné, Brazil and Leydolt twins, can be formulated as follows:

$$\text{Dauphine twin law: } 321 \Rightarrow 6'(3)22'$$
$$\text{Brazil twin law: } 321 \Rightarrow \bar{3}'(3)2/m'1(\bar{1}')$$
$$\text{Leydolt twin law: } 321 \Rightarrow \bar{6}'(3)2m' = 3/m'2m'.$$

Combination = 'complete twin': $6'(3)/m'2/m'2'/m'(\bar{1}')$; this symmetry corresponds to the hexagonal holohedral point group $6/m\,2/m\,2/m$, *cf.* Example 3.3.6.4.

(ii) Another example is provided by $KLiSO_4$ (crystal class 6), extensively investigated by Klapper *et al.* (1987):

$$\text{Inversion twins: } 6 \Rightarrow 6/m'(\bar{1}')$$
$$\text{Reflection twins: } 6 \Rightarrow 6m'm'$$
$$\text{Rotation twins: } 6 \Rightarrow 62'2'.$$

Combination = 'complete twin': $6/m'2'/m'2'/m'(\bar{1}')$; this symmetry is isomorphic to the complete-twin symmetry of quartz, given above, and to the hexagonal holohedral point group $6/m\,2/m\,2/m$.

(iii) An example of a very extensive series of pseudo-merohedral *growth twins* is provided by the zeolite minerals phillipsite and harmotome (Hoffmann *et al.*, 1973). Both minerals are monoclinic, space group $P12/m1$ (Rinaldi *et al.*, 1974). The crystals occur in series of pseudo-merohedral growth twins as follows:

$$1\,2/m\,1 \rightarrow 2'/m'\,2/m\,2'/m' \rightarrow 4'/m'\,2/m\,2'/m' \rightarrow 4'/m'\,\bar{3}'\,2/m.$$

The total subgroup index [*i*] from the monoclinic to the cubic twin symmetry is stepwise $2 \times 2 \times 3 = 12$. These steps are illustrated in the sketches of Fig. 3.3.6.16. If the gaps between the interpenetrating domains are filled, as in Fig. 3.3.6.16(*e*), the twin appears as a pseudo-cubic rhomb-dodecahedron.

3.3.7. Genetic classification of twins

In Section 3.3.3, a classification of twins based on their morphological appearance was given. In the present section, twins are classified according to their origin. Genetic terms such as growth twins, transformation twins and mechanical twins were introduced by Buerger (1945) and are in widespread use. They refer to the *physical origin* of a given twin in contrast to its geometrical description in terms of a twin law. The latter can be the same for twins of different origin, but it will be seen that the generation of a twin has a strong influence on the shape and distribution of the twin domains. An extensive survey of the genesis of all possible twins is given by Cahn (1954).

3.3.7.1. *Growth twinning*

Growth twins can occur in nature (minerals), in technical processes or in the laboratory during growth from vapour, melt or solution. Two mechanisms of generation are possible for growth twins:

(i) formation during nucleation of the crystal;

(ii) formation during crystal growth.

3.3.7.1.1. *Twinning by nucleation*

In many cases, twins are formed during the first stages of spontaneous nucleation, possibly before the sub-critical nucleus reaches the critical size necessary for stable growth. This idea was originally proposed by Buerger (1945, p. 476) under the name *supersaturation twins*. There is strong evidence for twin formation during nucleation for penetration and sector twins, where all domains originate from one common well defined 'point' in the centre of the twinned crystal, which marks the location of the spontaneous nucleus.

Typical examples are the *penetration twins* of iron borate $FeBO_3$ (calcite structure), which are intergrowths of two rhombohedra, a reverse and an obverse one, and consist of 12 alternating twin domains belonging to two orientation states (see Example 3.3.6.6 and Fig. 3.3.6.6). Experimental details are presented by Klapper (1987) and Kotrbova *et al.* (1985). Further examples are the penetration twins of the spinel law (Example 3.3.6.7 and Fig. 3.3.6.8), the very interesting and complex [001] penetration twin of the monoclinic feldspar orthoclase (Fig. 3.3.7.1) and the *sector twins* of ammonium lithium sulfate with three orientation states (Fig. 3.3.7.2).

It should be emphasized that *all* iron borate crystals that are nucleated from flux or from vapour (chemical transport) exhibit penetration twinning. The occurrence of untwinned crystals has not been observed so far. Crystals of isostructural calcite and $NaNO_3$, on the other hand, do not exhibit penetration twins at all. In contrast, for ammonium lithium sulfate, NH_4LiSO_4, both sector-twinned and untwinned crystals occur in the same batch. In this case, the frequency of twin formation increases with higher supersaturation of the aqueous solution.